*Quart. J. R. Met. Soc.* (1983), **109**, pp. 81–111 551.509.333:551.224.735

# Numerical forecasts of stratospheric warming events using a model with a hybrid vertical coordinate

By A. J. SIMMONS and R. STRÜFING
*European Centre for Medium Range Weather Forecasts, Shinfield Park, Reading, Berks, U.K.*

(Received 17 February 1982; revised 1 June 1982)

SUMMARY

A numerical forecast model based on use of a hybrid vertical coordinate which is terrain-following at low levels but which tends continuously to a pressure coordinate at upper levels is introduced. Results from this model are first presented for 10-day forecasts (extending up to 10 mb) of the major stratospheric circulation changes which occurred during the winter of 1979. A considerable degree of success is illustrated, not only in predicting a major wavenumber-two warming up to 10 days ahead, but also in the forecasting of a preceding development of wavenumber one and a subsequent decay of the wavenumber two perturbation. Diagnosis using Eliassen-Palm cross-sections confirms previous observational diagnoses and aids understanding of the performance of the forecast model. Computations of the meridional gradient of zonal-mean potential vorticity are also discussed.

The sensitivity of tropospheric forecasts to stratospheric resolution and the choice of vertical coordinate is also examined. These forecasts are in fact characterized by a marked insensitivity to such aspects. Thus lowering the top forecast level from 10 mb to 50 mb has little effect on objective forecast scores averaged over the extratropical troposphere of the Northern Hemisphere, although planetary-wave structures in high latitudes are affected to a small degree. The hybrid coordinate gives results similar to those obtained using the usual sigma coordinate, but such differences as are found tend to favour the use of the hybrid representation. Idealized analyses of the stability of the semi-implicit time scheme for hybrid coordinates are confirmed in practice.

## 1. INTRODUCTION

This paper is intended to serve two main purposes. The first is to present a series of noteworthy numerical forecasts of the substantial stratospheric circulation changes that took place during January and February, 1979. The second is to discuss the corresponding tropospheric forecasts obtained using several different vertical resolutions in the stratosphere and two different vertical coordinate systems.

The numerical forecast model used for these experiments is a modified version of the global, primitive-equation model used for operational prediction at the European Centre for Medium Range Weather Forecasts. A previous attempt at such a numerical forecast of a stratospheric warming (for March, 1965) was reported by Miyakoda *et al.* (1970). These authors achieved some success in predicting a splitting of the circumpolar vortex, but failed to simulate the observed polar warming. Subsequently, models in which quite realistic stratospheric warmings occur as a result of a prescribed, idealized tropospheric forcing have been developed (Matsuno, 1971; Holton, 1976), and more recently warmings have been found to arise spontaneously in numerical simulations of the general circulation of the troposphere and stratosphere (O'Neill, 1980; Grose and Haggard, 1981). In addition, the period since Miyakoda *et al.*'s experiments has seen a substantial improvement in the accuracy with which the larger scales of tropospheric motion may be forecast (Bengtsson and Simmons, 1983).

The present experiments were facilitated by a fortunate coincidence. One of the features of the atmospheric circulation during the year of the First GARP Global Experiment (FGGE) was a period during January and February in which large stratospheric changes took place. Most notable was a major warming of the relatively rare 'wavenumber two' type which took place during the latter half of February.

A good review of the dynamics of stratospheric warmings, with particular emphasis on the winter of 1979, has been given by McIntyre (1982). The present results complement both diagnostic studies, such as those by Quiroz (1979) and Palmer (1981), and more mechanistic modelling studies such as that by Butchart *et al.* (1982). The latter paper shows how the wavenumber two warming may be forecast using the observed 100 mb geopotential field as the forcing of the stratosphere. It also presents an illuminating sequence of experiments clarifying the mechanism of the warming. Here we show how the

warming may be forecast up to at least 10 days in advance using a combined tropospheric/stratospheric model. We also present the forecast of an earlier wavenumber one warming whose importance has been discussed by Labitzke (1981), and the forecast of the re-establishment of a single stratospheric vortex at the beginning of March, 1979.

In view of the significant interactions between troposphere and stratosphere known to take place at times of stratospheric warming, these cases are also used to examine the sensitivity of the tropospheric forecasts to the numerical representation of the stratosphere. The bulk of results are presented for hybrid vertical coordinate surfaces which follow the model orography at low levels, but which gradually flatten to become surfaces of constant pressure in the stratosphere. The top ('full') level at which winds and temperature are forecast is 10 mb. A general vertical finite-difference scheme and discussion of the possible advantages of such coordinates have been given by Simmons and Burridge (1981). In the latter part of the present paper we compare the hybrid-coordinate results for a 10 mb top (full) level with those for lower top levels of 25 and 50 mb respectively. We also compare these results with those obtained using the traditional sigma coordinate (Phillips, 1957).

Details of the numerical model are given in the following section, and the initial and verifying data are discussed in Section 3. The reader interested mainly in the results themselves may turn directly to Section 4, where the stratospheric forecasts made using the resolution which extends to 10 mb are presented and discussed. Sensitivity to the numerical representation forms the subject matter of Section 5.

## 2. The numerical model

The numerical model chosen for the first phase of operational forecasting at ECMWF uses a horizontal finite-difference scheme based on a staggered grid of variables known as the C-grid (Arakawa and Lamb, 1977). Choice of this grid was made mainly because of its low computational noise and the ease of implementation of a semi-implicit time scheme. The grid interval is 1·875° of latitude and longitude. Following the work of Arakawa (1966) and Sadourny (1975), the finite difference scheme was designed to conserve potential enstrophy during vorticity advection by the horizontal flow. Further detail has been given by Burridge and Haseler (1977), and Burridge (1979). The related parametrization scheme (Tiedtke *et al.*, 1979) describes the interactions thought to be of importance in the medium range, including a full hydrological cycle, a relatively detailed stability-dependent representation of boundary and free-atmospheric turbulent fluxes, and an interaction between the radiation and model-generated clouds.

For this study, the general vertical finite-difference scheme described by Simmons and Burridge (1981) has been included in the forecast model. Precise details are not of importance in the present context, but we note that the form for the calculation of the geopotential at the top model level is that given by Eq. (3.19) of Simmons and Burridge's paper, and the corresponding definition (3.18) of full-level pressure is adopted. The sigma-coordinate horizontal difference scheme described by Burridge and Haseler (1977) is generalized in a natural way, a sigma-coordinate term such as

$$\{\overline{(p_s u_k \delta_\lambda T_k)}^{\lambda}\}/p_s$$

at level $k$ becoming

$$\{\overline{(\Delta p_k u_k \delta_\lambda T_k)}^{\lambda}\}/\Delta p_k .$$

Here $p_s$ is the surface pressure, $u_k$ and $T_k$ the zonal velocity and temperature at level $k$, and $\Delta p_k$ the pressure difference across the model layer containing the $k$th level. The operators $\overline{(\ )}^{\lambda}$ and $\delta_\lambda$ have their usual meanings. Complete details will not be given here but we note that the general scheme reproduces Burridge and Haseler's horizontal scheme in the

special case of sigma coordinates, and that the conservation properties of the horizontal scheme for general coordinates are the same as those for sigma coordinates.

The philosophy behind the implementation of the new scheme was to produce, for the purposes of initial research, as general a scheme as possible with a minimum of recoding of the operational model. Thus the physical parametrizations coded for sigma coordinates were implemented by defining, for each grid-point of the model, a local sigma coordinate with a resolution such that the sigma levels coincided with the general coordinate surfaces at the point in question. A result of this philosophy is that the more general model carries a computational overhead of some 20% when compared with the operational model. It must be stressed, however, that careful program design, restriction to a coordinate of the form given by Eq. (1) below, and coding to omit terms which are zero for coordinate surfaces which are surfaces of constant pressure, should result in a substantially reduced overhead. Indeed, preliminary results of such an exercise suggest an increase in cost of only about 2% for the type of resolution used here. A hybrid model in which the majority of levels are levels of constant pressure, for example a model designed for predominantly stratospheric and mesospheric studies, should prove more efficient than a corresponding sigma coordinate model.

A feature of the difference scheme described by Simmons and Burridge (1981) is that an explicit definition of the vertical coordinate is not required. Rather, it is necessary only to specify the pressure of each model level as a function of the surface pressure. Most results presented here are for a simple generalization of the sigma coordinate for which the pressures at model 'half' levels are given by

$$p_{k+1/2} = A_{k+1/2} + B_{k+1/2}\, p_s, \quad k = 0, 1, 2, \ldots \text{NLEV} \tag{1}$$

with $A_{1/2} = B_{1/2} = A_{\text{NLEV}+1/2} = 0$ and $B_{\text{NLEV}+1/2} = 1$.

This form of coordinate is particularly efficient from a computational viewpoint, and allows a direct control over the "flattening" of coordinate surfaces as the pressure decreases, since the $A$'s and $B$'s may be determined by specifying the distribution of model pressure levels for a typical sea level surface pressure and for a surface pressure typical of the lowest expected to be attained in the model.

Results will be presented from 18-, 16- and 14-level calculations. Full-level pressures are given in Table 1 for a surface pressure of 1013·2 mb. 16-level calculations have been

TABLE 1. FULL-LEVEL PRESSURES IN mb FOR 14, 16 AND 18 LEVEL RESOLUTIONS FOR A SURFACE PRESSURE OF 1013·2 mb

| NLEV | | |
|---|---|---|
| 14 | 16 | 18 |
| | | 10 |
| | | 33 |
| | 25 | 65 |
| | 77 | 105 |
| 50 | 136 | 154 |
| 145 | 200 | 211 |
| 241 | 270 | 276 |
| 331 | 345 | 348 |
| 419 | 423 | 425 |
| 505 | 506 | 506 |
| 591 | 590 | 590 |
| 675 | 673 | 673 |
| 755 | 754 | 754 |
| 830 | 830 | 830 |
| 897 | 896 | 896 |
| 951 | 951 | 951 |
| 990 | 990 | 990 |
| 1009 | 1009 | 1009 |

performed for both hybrid and sigma coordinates, with the coordinate surfaces coinciding for the pressure of 1013·2 mb. The hybrid coordinates all reduce exactly to pressure coordinates for full-level pressures lower than 100 mb.

The variation of selected coordinate surfaces with varying surface pressure is illustrated in Fig. 1 for the four cases considered. In general, values of $A_{k+1/2}$ and $B_{k+1/2}$ in Eq. (1) may be adjusted to give more or less flat coordinate surfaces over high ground, and in practice a balance must be found between the desirability of having coordinate surfaces as close as possible to pressure surfaces and the possible disadvantages in computational stability and accuracy associated with the consequential fine, and rapidly-varying, low-level vertical resolution over mountains.

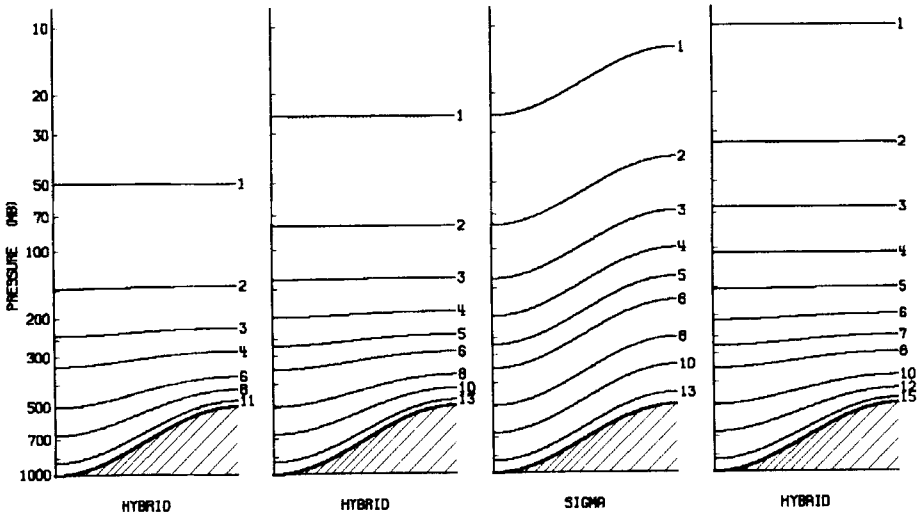


Figure 1. The variation of selected coordinate surfaces with surface pressure for hybrid and sigma coordinates. The location of levels for a surface pressure of 1013·2 mb is given in Table 1.

## 3. Initial and verifying data

The dramatic evolution of the 1979 wavenumber-two warming occurred within a few days of February 20, with a single cyclonic vortex re-established during the early days of March. The preceding wavenumber one warming began in mid-January. As sigma-coordinate forecasts from 00GMT data for 16 January and 17 February had already been the subject of study at ECMWF, these initial dates and times were also chosen for the present experiments. Forecasts from 00GMT on 9, 13, 21 and 25 February were also performed in order to examine the immediate pre- and post-warming phases of the later event.

Initial data were constructed for the hybrid vertical coordinate by interpolating analysed, pressure-level data to the model levels. Routines for interpolation from pressure to sigma used operationally until December 1980 were modified to achieve this. Non-linear normal-mode initialization routines (Temperton and Williamson, 1981; Williamson and Temperton, 1981) were also modified to run with the general coordinate, using modes calculated as indicated in Section 4 of the paper by Simmons and Burridge (1981). These routines have not, however, been used here for initial data since gravity-wave amplitudes have been generally found to be initially little more than 1 mb in surface pressure and to decay to negligible values over the first day or so of integration.

Many of the routines used at ECMWF for the display, diagnosis and verification of forecast results use a post-processed form of forecast data which has been interpolated from sigma coordinates to standard pressure levels. Post-processing routines were accordingly modified to transform forecast data from the hybrid coordinate surfaces to the standard pressure levels.

Initial pressure-level data were derived either from the standard 'Level IIIb' FGGE analyses produced at ECMWF (Bengtsson *et al.*, 1982a), or from modified FGGE analyses produced using more recent revisions of the data assimilation scheme. It should be noted that the analyses were derived from data assimilation cycles which used a standard sigma-coordinate model, and the experiments reported here thus do not test the full impact that use of a hybrid coordinate might have when incorporated in a complete forecasting system.

Verifying stratospheric analyses were also taken from the Level IIIb analyses. These were initialized using the hybrid vertical coordinate extending up to 10 mb, the top level of the analysis, in order to reduce a small degree of roughness present in the uninitialized analyses. This roughness rapidly disappears in the course of the corresponding forecasts. The largely cosmetic nature of this modification of the stratospheric analysis is confirmed by the generally good agreement between forecasts and verifying analyses. For the objective tropospheric verification of the forecasts, analyses produced independently by the Deutscher Wetterdienst were used.

## 4. Stratospheric forecasts

### (*a*) *Synoptic maps*

We first discuss a selection of maps of the height of the 10 and 50 mb pressure surfaces, and begin with the forecast of the wavenumber 2 warming using the initial analysis for 17 February. Maps from this analysis are presented in Fig. 2, which shows

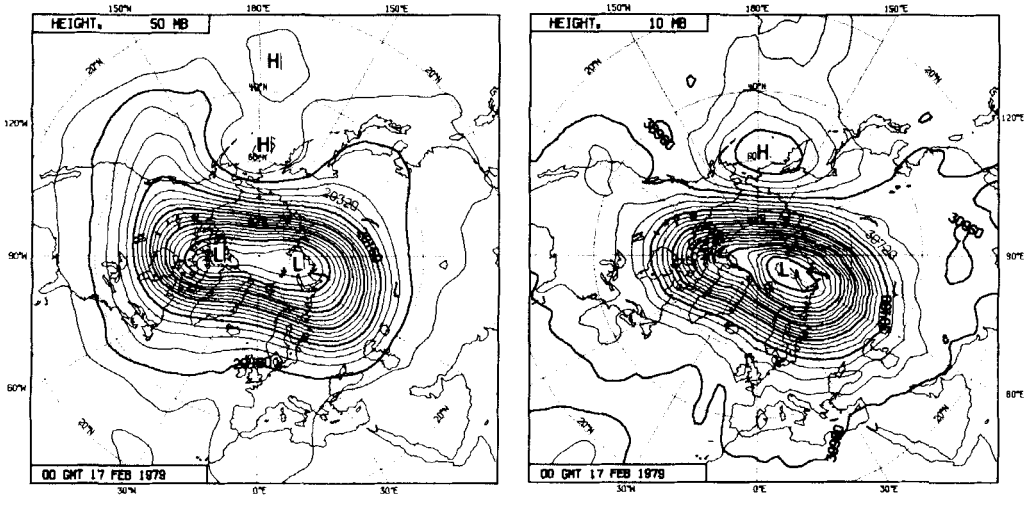


Figure 2. Northern-hemispheric maps of the height (m) of the 50 mb (left) and 10 mb (right) pressure surfaces for 17 February, 1979. The contour interval is 80 m at 50 mb and 120 m at 10 mb.

that by this date elongation of the stratospheric vortex had begun, with two low centres evident at 50 mb. At 10 mb, the splitting of the vortex is less evident, and the Aleutian High more clearly defined.

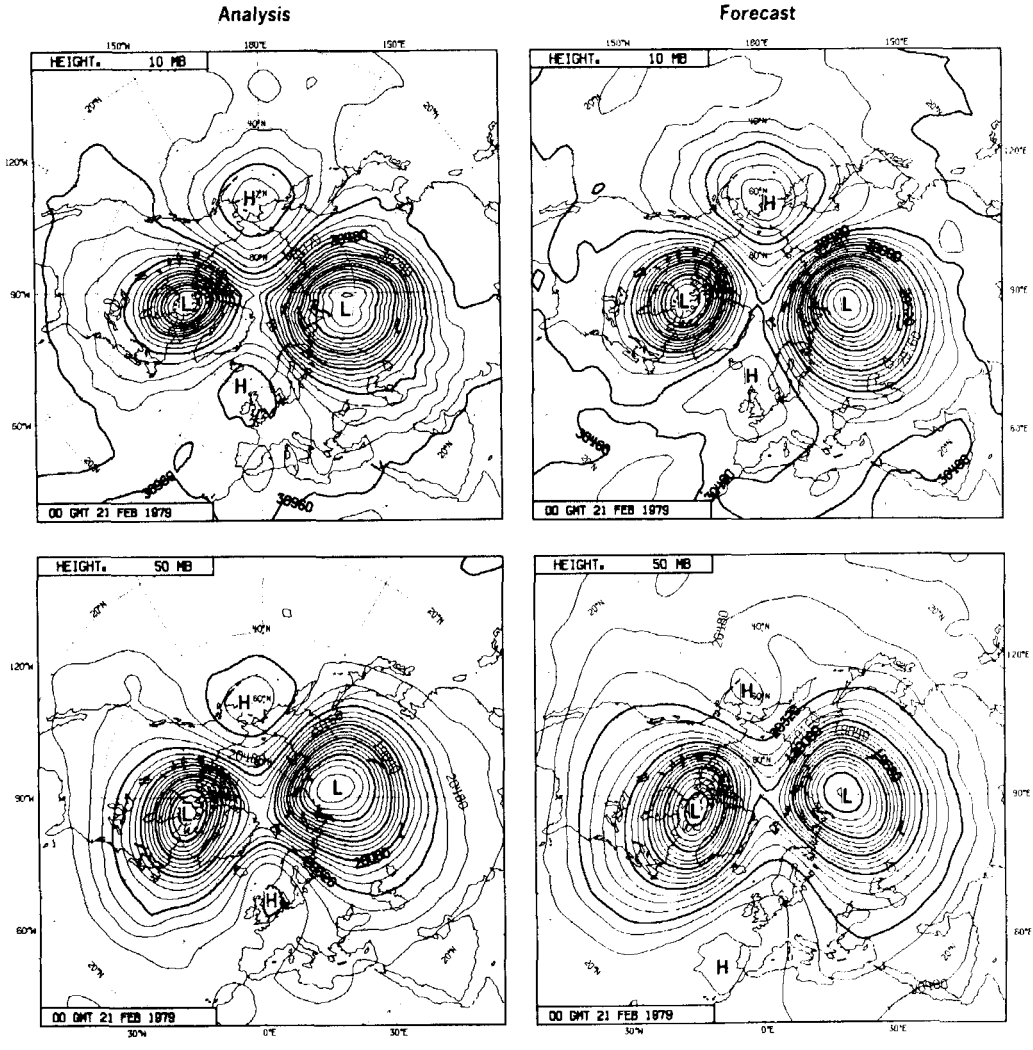


Figure 3. Maps of 10 mb (upper) and 50 mb (lower) heights for 21 February (left) and for forecasts from 17 February (right).

Figure 3 shows that a dramatic change has taken place, and been correctly forecast, over the next four days. Two separate cyclonic vortices of approximately equal intensity have formed by 21 February, and ridges of high pressure extend towards the pole, asymmetry again being more pronounced at 10 mb where the Aleutian High is more marked than the high over Europe. The accuracy of the forecast is such that little needs to be written about it. We note that the lower absolute heights of the forecast fields reflect a general cooling which is a characteristic feature of the forecast model (Bengtsson and Simmons, 1983).

Forecast deficiencies are more evident at day 8, as is shown in Fig. 4. The 10 mb forecast remains quite successful, the model capturing a retrogression of the wave pattern and extension of high pressure over the pole, although the Aleutian High is too strong, and displaced towards the west. At 50 mb, however, there is a substantial erroneous weakening of the individual cyclonic circulations, and an erroneous strengthening of the

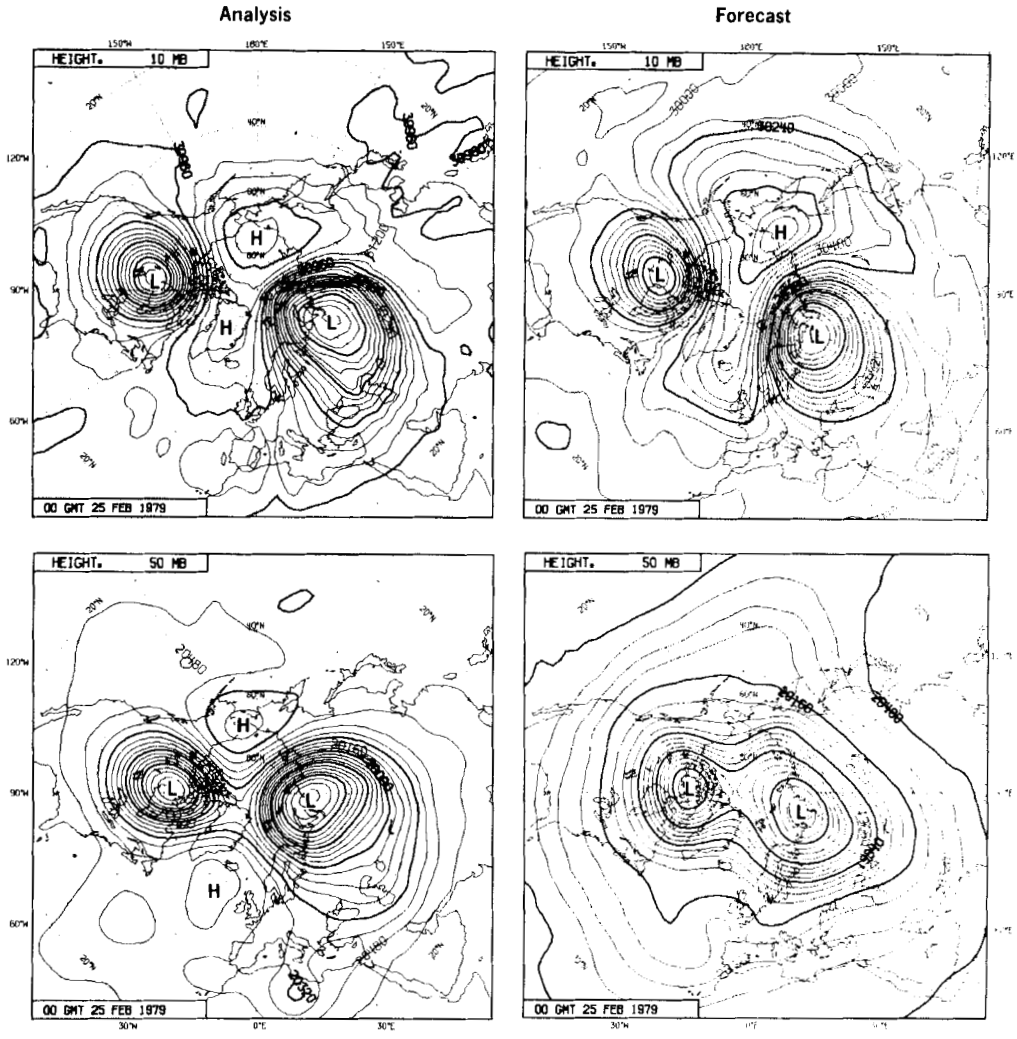


Figure 4. Maps of 10 mb (upper) and 50 mb (lower) heights for 25 February (left) and for forecasts from 17 February (right).

zonal-mean component of the flow. It will later be shown that this particular case is one with a relatively poor tropospheric forecast, and evidence will be discussed which suggests that tropospheric error spreads upward to influence seriously the 50 mb forecast, but not the 10 mb forecast, by day 8. A much more successful 8-day (and 10-day) forecast of the vortex split at 50 mb, starting earlier from 12 February, is shown by Bengtsson *et al.* (1982b).

Initial 50 and 10 mb heights for the forecast from 16 January are shown in Fig. 5. As on 17 February, some disturbance of the stratospheric circulation is evident, with again two separate low centres. A major difference lies in the meridional extent of the circulation, which is substantially larger at the earlier date. A wavenumber 3 component of the height field is also quite marked at this time.

Analysed fields for 24 January, and the 8-day forecast from 16 January, are shown in Fig. 6. Marked changes in circulation have again taken place and been largely captured

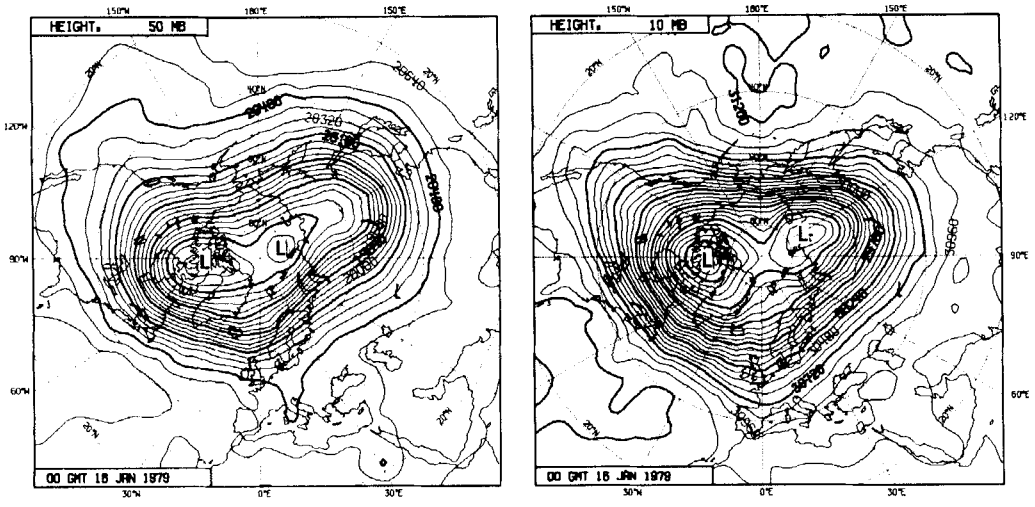


Figure 5. Maps of 50 mb (left) and 10 mb (right) heights for 16 January, 1979.

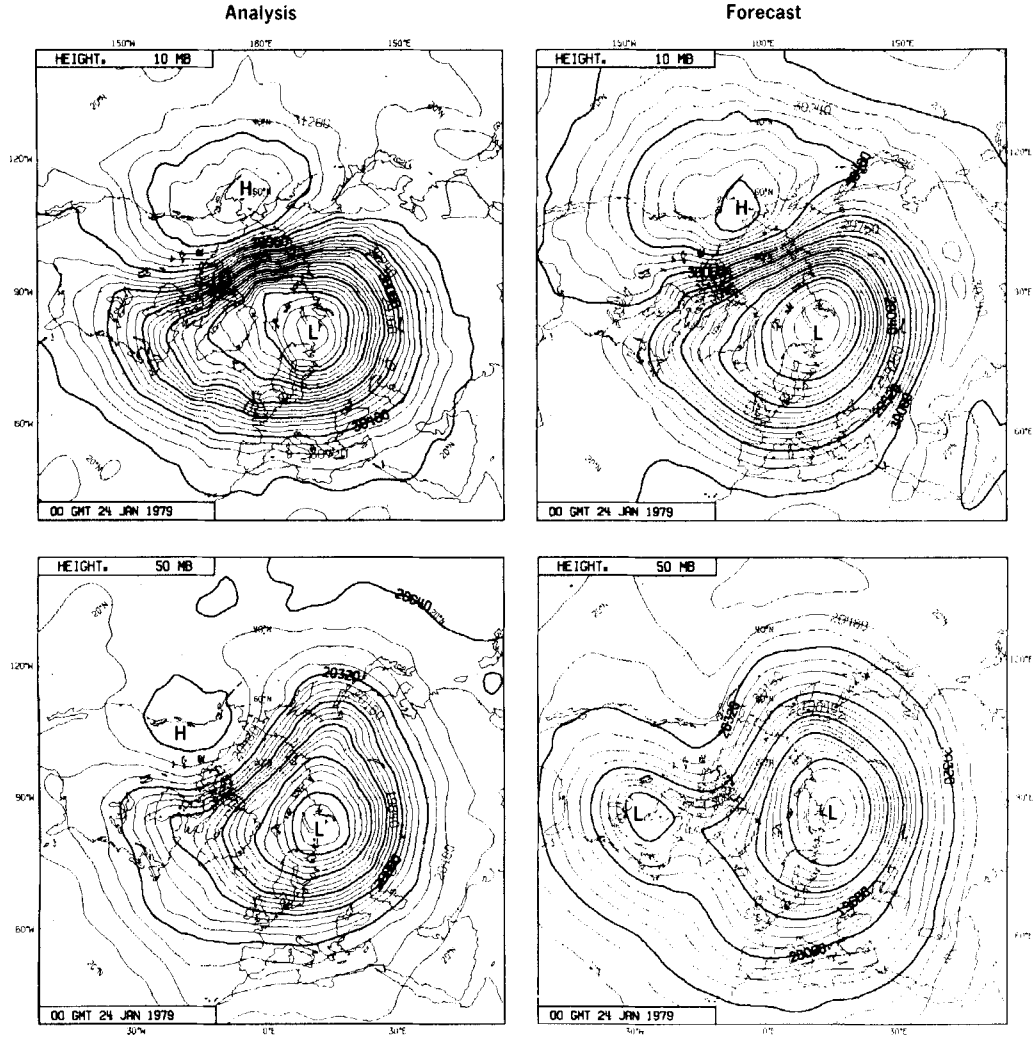


Figure 6. Maps of 10 mb (upper) and 50 mb (lower) heights for 24 January (left) and for the forecast from 16 January (right).

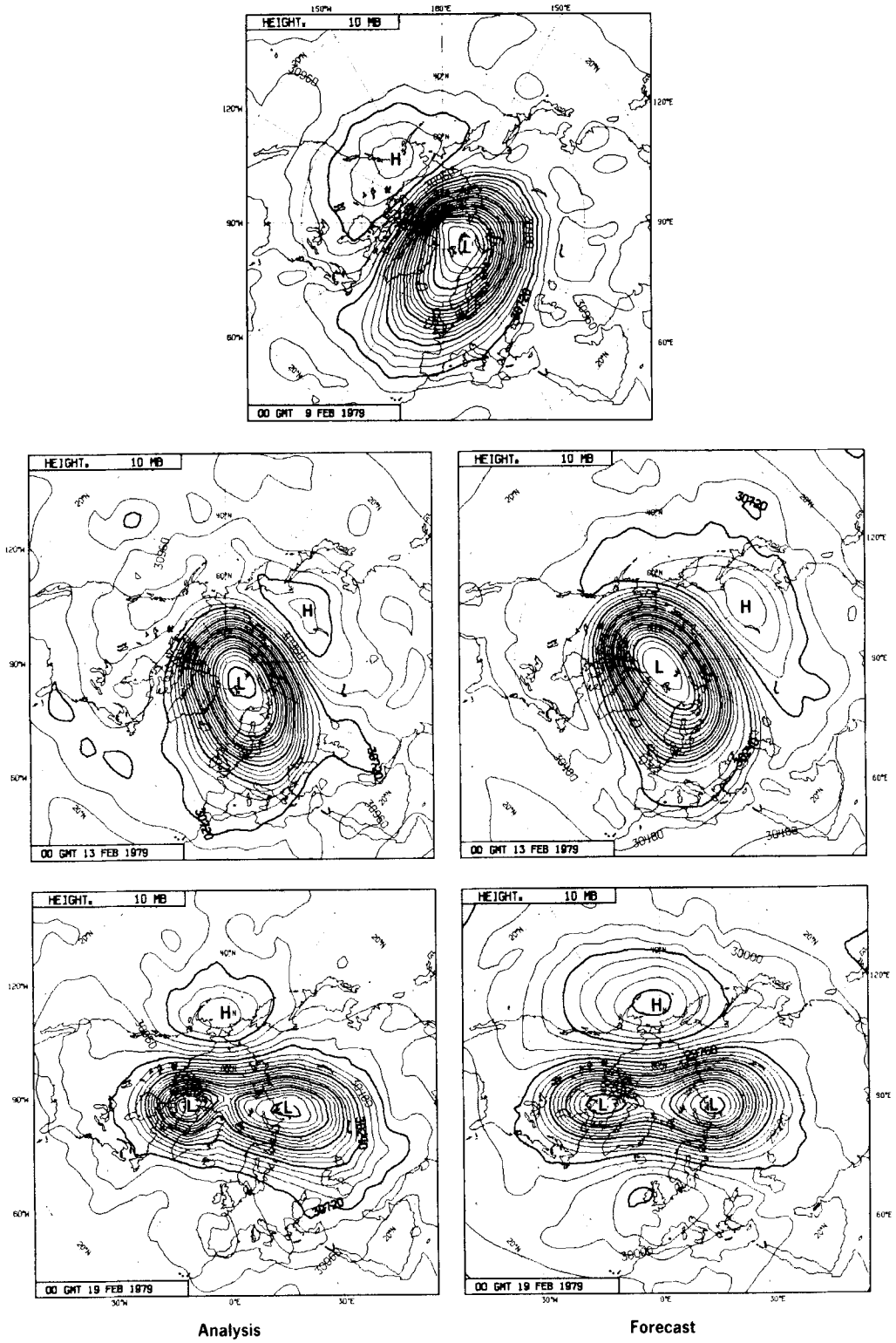


Figure 7. Maps of the 10 mb height for 9 February (upper), 13 February (middle left) and 19 February (lower left). 4- and 10-day forecasts from 9 February are also shown.

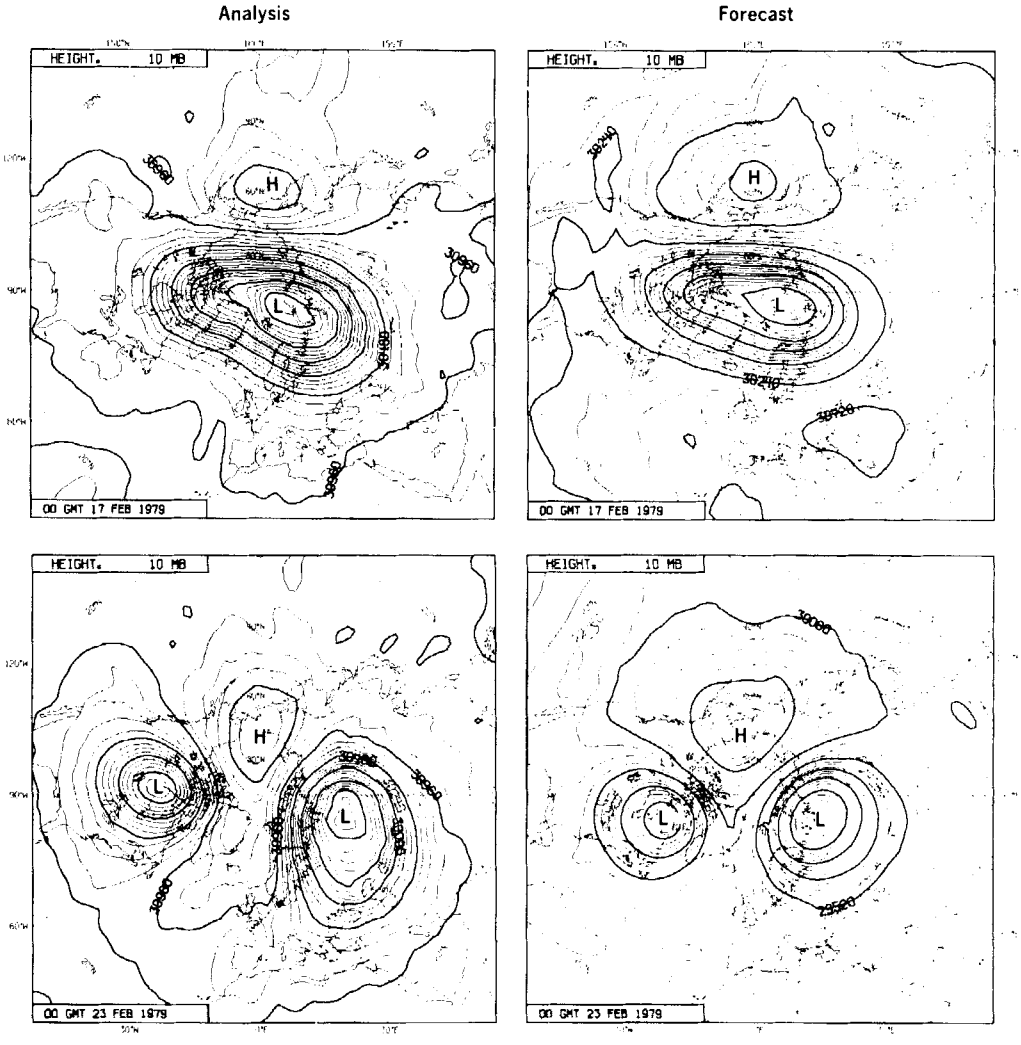


Figure 8. Maps of the 10 mb height for 17 February (upper left) and 23 February (lower left). 4- and 10-day forecasts from 13 February are also shown.

by the forecast. A pronounced development in wavenumber one has occurred, with strong cross-polar flow. At 10 mb the Aleutian High is again forecast to be too intense, while at 50 mb confinement of the flow towards polar regions is underestimated and the trough near 90°W exaggerated. The overall evolution of the stratospheric circulation has, however, been described in the forecast.

Figures 7, 8 and 9 present 10 mb forecasts from additional dates within February, 1979. Figure 7 shows the initial state for 9 February, together with 4- and 10-day forecasts and corresponding analyses. Between the 9th and 13th a marked change in orientation of the main vortex occurs while the Aleutian High weakens and moves eastward, a new high

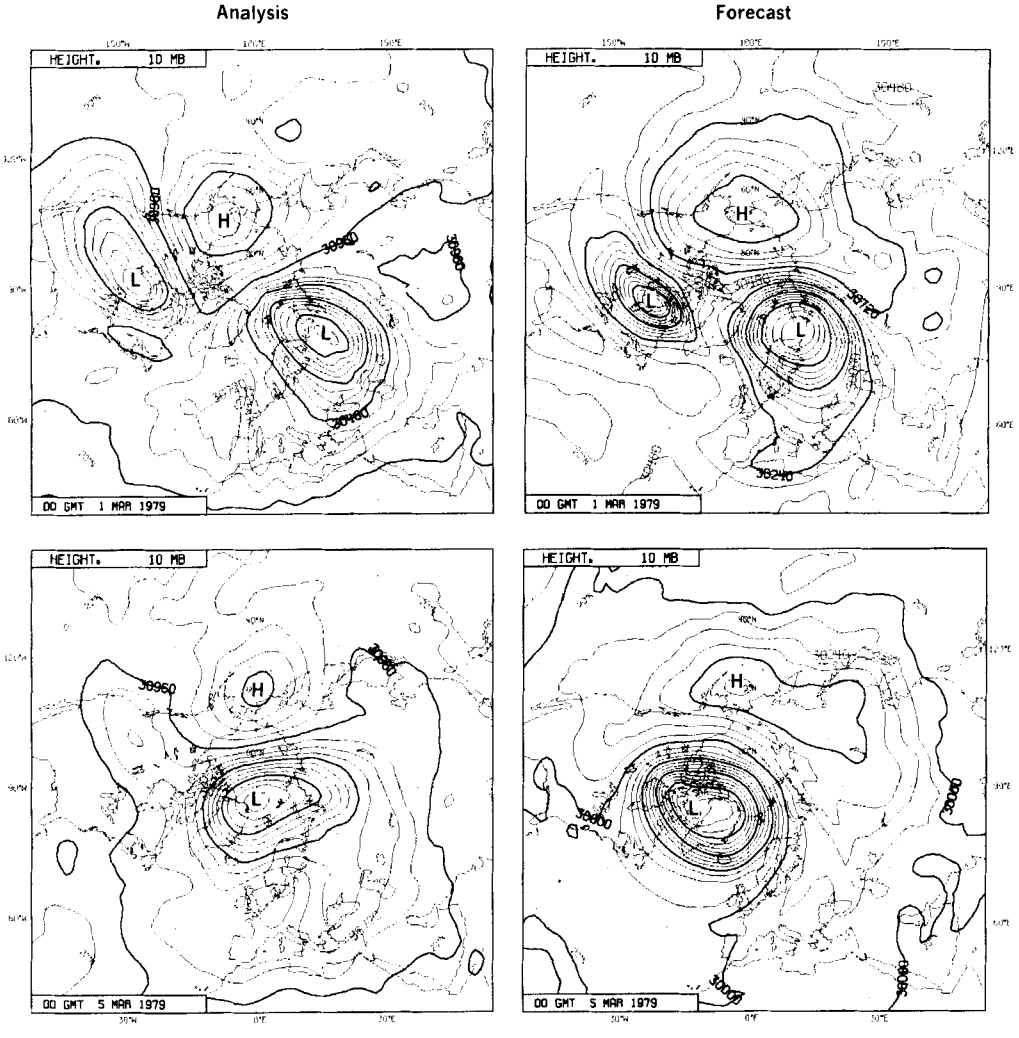


Figure 9. Maps of the 10 mb height for 1 March (upper left) and 5 March (lower left). 4- and 8-day forecasts from 25 February are also shown.

developing over eastern Asia. By the 19th splitting of the vortex has clearly begun, and the new high has amplified and moved close to the date line. These quite substantial changes prior to the peak of the warming may be seen to be well represented throughout the 10-day forecast period.

Four- and 10-day forecasts from 13 February are shown in Fig. 8. By 23 February the splitting of the vortex has completely occurred, both in reality and in the notably accurate 10-day forecast. Overintensification of the Aleutian High is yet again evident, as indeed it is in Fig. 7.

The final synoptic example is from the initial state for 25 February which was shown in Fig. 4. The 4-day forecast shown in Fig. 9 successfully captures a weakening of the

high pressure in the immediate vicinity of the pole, and the development of a marked horizontal tilt to the low pressure pattern over North America. This low more or less disappears over the following four days both in reality and in the forecast. Thus the 8-day forecast reproduces the change from two cyclonic circulations of approximately equal intensity to one principal off-centred vortex, although the strength of the latter is overestimated, and its position is also in error.

### (*b*) *Zonal-mean zonal winds*

The generally successful nature of the stratospheric forecasts illustrated by the height maps is confirmed by examination of meridional cross-sections of the zonal-mean component of the zonal wind. Figure 10 presents such a section for 16 January, together with

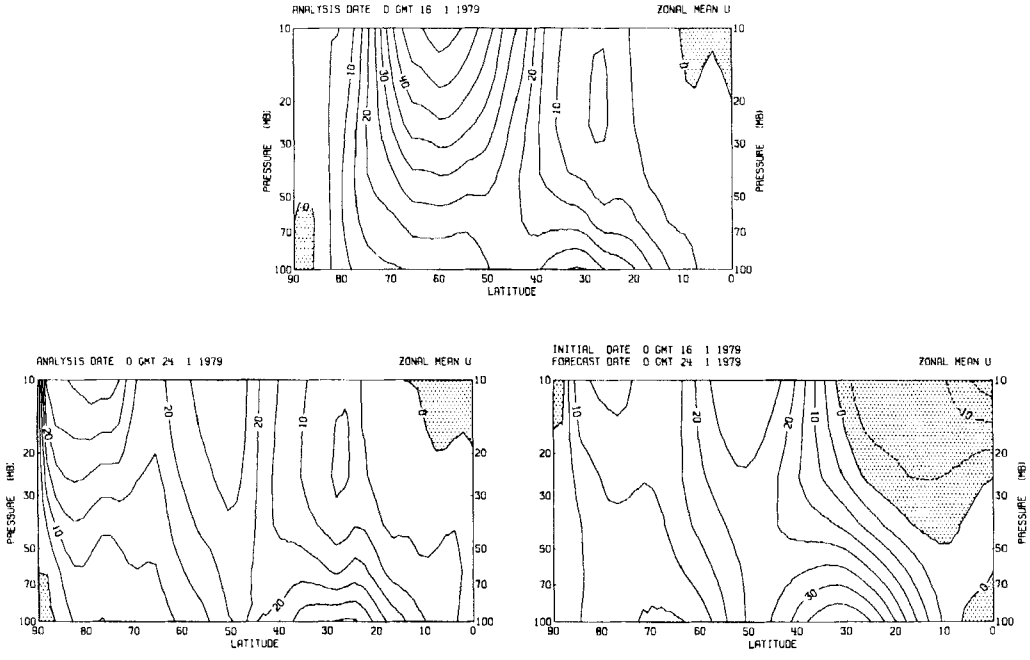


Figure 10. Meridional cross-sections of the zonal-mean zonal wind ($m\,s^{-1}$) for 16 January (upper) and 24 January (lower left). The 8-day forecast from 16 January is also shown. The contour interval is $5\,m\,s^{-1}$ and regions of easterly flow are shaded.

that for the 8-day forecast from this date and the corresponding analysis. It shows the forecast to have successfully described a marked weakening of the initial, relatively broad and strong, westerly jet, although in neither the forecast nor the analysis for this date has the circulation reversed.

Errors of detail may be seen in the 8-day forecast. In this particular case the westerly zonal-mean flow close to the pole is underestimated, while errors in the tropics and subtropics are more systematic in nature, as may be seen by comparison with Figs. 11 and 12. Examination of the 100 mb flows indicates the too strong subtropical jet which characterizes the ECMWF model (Hollingsworth *et al.*, 1980; Bengtsson and Simmons, 1983), while the excessive poleward extension of the tropical easterly flow in the middle stratosphere may be linked with an erroneous cooling of this region which is discussed further in sub-section (*e*).

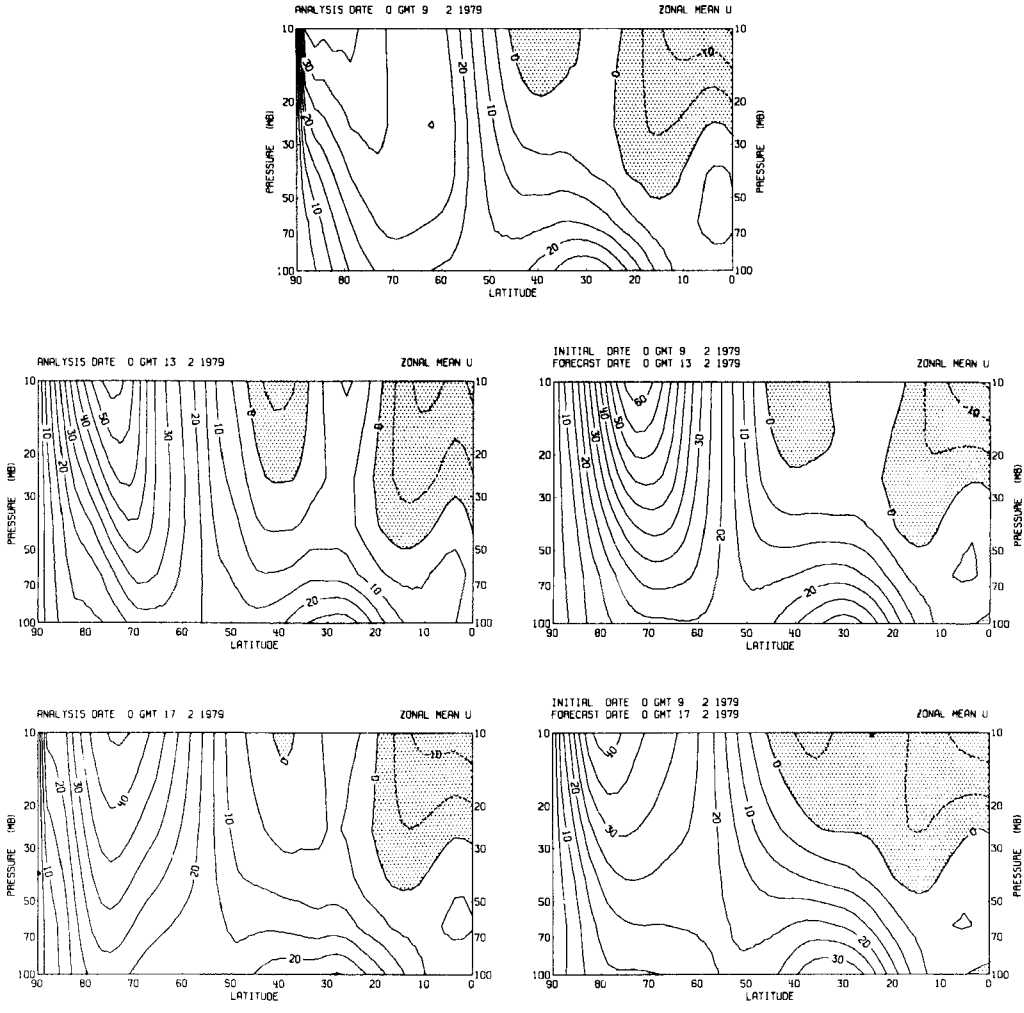


Figure 11. Meridional cross-sections of zonal-mean zonal wind for 9 February (upper), 13 February (middle left) and 17 February (lower left). 4- and 8-day forecasts from 9 February are also shown.

Notwithstanding these systematic errors, Figs. 11 and 12 also exhibit generally successful forecast results. The forecast from 9 February shown in Fig. 11 clearly describes a substantial initial strengthening of the zonal-mean flow, and then a weakening as the wavenumber-two warming event begins. Figure 12 shows 8-day forecasts from the 13th, 17th and 25th February, together with verifying analyses. The former two of these (for which initial cross-sections may be found in Fig. 11) illustrate the successful predictions of the circulation reversal which occurs first close to the North Pole and then spreads towards the equator. The forecast from the later date describes the re-establishment of the westerly polar circulation at all levels in the middle and lower stratosphere.

### (*c*) *Eliassen-Palm cross sections*

It has been suggested by Edmon *et al.* (1980) that the so-called 'Eliassen-Palm Cross Section' is a useful diagnostic of wave motion and the interaction of this motion with the zonal-mean state. Such sections are discussed here with three main purposes in mind. The first is to illustrate the general agreement between sections computed from forecast and

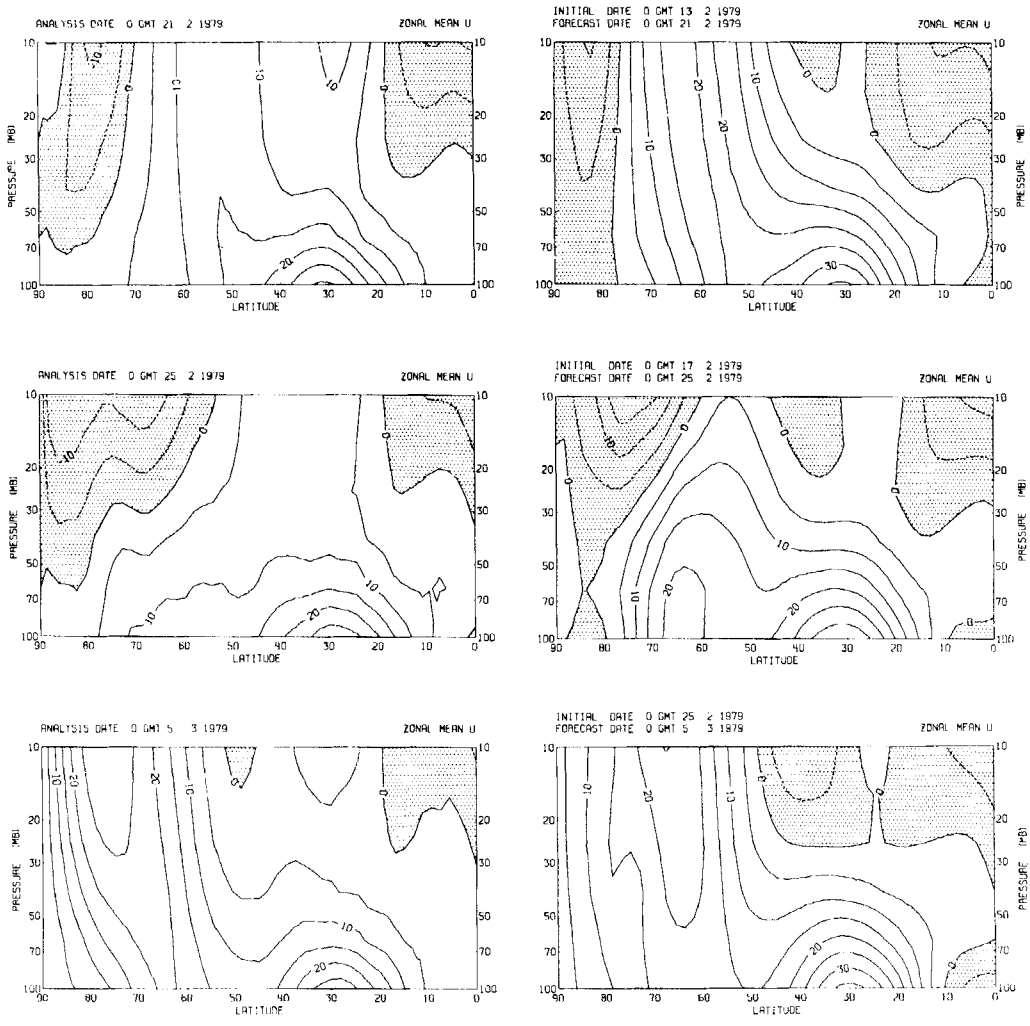


Figure 12. Meridional cross-sections of zonal-mean zonal wind for 21 February (upper left), 25 February (middle left) and 5 March (lower left). 8-day forecasts verifying on these dates are shown in the right-hand sections.

analysed data, an agreement which gives confidence in the picture of reality revealed both by these analyses and by the independent analyses discussed by Palmer (1981). The second is to illustrate the extent to which the amplitude of the Eliassen-Palm flux is smaller in the stratosphere than in the troposphere, a result which relates to our subsequent discussion of the extent to which the tropospheric forecasts are sensitive to stratospheric resolution. Thirdly, these sections are used to aid discussion of the relatively poor day 8 forecast from 17 February shown in Fig. 4.

The form of meridional section adopted here is that recommended by Edmon *et al.* (1980) when the logarithm of pressure is used as the vertical scale in the sections. The flux vector, $\hat{\mathbf{F}}$, with components $\hat{\mathbf{F}}_\theta$ and $\hat{\mathbf{F}}_p$ proportional to the horizontal eddy fluxes of momentum and heat, is given by

$$(\hat{\mathbf{F}}_\theta, \hat{\mathbf{F}}_p) = -\frac{2\pi a^2}{g}\cos^2\theta\left(p\,\overline{u'v'}, fa\frac{\overline{v'T'}}{S}\right). \tag{2}$$

Here $\theta$ is latitude, $p$ is pressure, $u'$ is the eddy zonal velocity, $v'$ the eddy meridional velocity, $T'$ the eddy temperature, $a$ the radius of the earth, $f$ the Coriolis parameter and $g$ the acceleration due to gravity. The static stability $S$ is given by

$$S = \frac{\kappa \bar{T}}{p} - \frac{\partial \bar{T}}{\partial p},$$

where $\bar{T}$ is the zonal-mean temperature and $\kappa$ denotes, as usual, $R/c_p$, the gas constant divided by the specific heat at constant pressure. Contours of the divergence of the Eliassen-Palm flux, given by

$$\nabla \cdot \mathbf{F} = -\frac{1}{a\cos\theta}\frac{\partial}{\partial\theta}\left(\cos^2\theta\,\overline{u'v'}\right) - f\cos\theta\,\frac{\partial}{\partial p}\left(\frac{\overline{v'T'}}{S}\right) \tag{3}$$

are also shown. The scaling of the flux vector is such that the pattern of arrows looks non-divergent only when $\nabla \cdot \mathbf{F} = 0$.

As discussed in Edmon *et al.*'s paper (and also earlier by Andrews and McIntyre, 1976, 1978; and Boyd, 1976), the term given by Eq. (3) describes, to the accuracy of quasi-geostrophic theory, the sole forcing of changes to the zonal-mean state by the wave motion. More specifically, the term represents a forcing of the zonal-mean zonal wind although in general it will not give the acceleration that actually occurs because of the presence of an additional term in the equation for this zonal-mean wind. This term, representing the effect of a 'residual mean meridional circulation', ensures that the actual change in the zonal-mean wind is accompanied by a change in the zonal-mean temperature such as to preserve thermal-wind balance.

Figure 13 presents Eliassen-Palm cross-sections for 20 January, 1979. The upper plot is computed from the objective stratospheric analysis, while the middle section is that from the 4-day forecast from 16 January. Agreement is generally good, fluxes being somewhat smaller in the forecast, and flux divergences and convergences appearing rather rough in the analysis. Fluxes are generally directed upward and equatorward, in a pattern characteristic of the winter stratosphere, although magnitudes are larger by a factor of about three than computed for the climatological January standing-wave pattern. The flux convergence is a maximum between 50° and 60°N, at a latitude close to that of the maximum zonal flow reduction indicated by Fig. 10 for the period 16–24 January.

The lower section in Fig. 13 shows a combined section for the troposphere and stratosphere for the 4-day forecast. The corresponding section for the analysis is very similar in essential detail, and is not shown. Although the stratosphere was undergoing a substantial change at this time, it is noteworthy that the magnitude of the Eliassen-Palm flux is substantially larger in the troposphere than in the stratosphere.

Stratospheric sections from the analysis for 21 February and from the 4-day forecast verifying on this date are presented in Fig. 14. Both sections show a strong upward flux (note the change of scale from Fig. 13), with a poleward component north of about 60°N. The flux is convergent over almost all the lower and middle stratospheric region shown. At this and other days, there is overall agreement with sections published by Palmer (1981, Fig. 3). An exception is a failure to predict a temporary re-establishment of the poleward flux in 1- and 5-day forecasts verifying on February 26, although the success of the forecast from February 25 shown in Fig. 9 suggests that this failure is of little significance.

It is also instructive to examine sections for the combined troposphere and stratosphere for the case shown in Fig. 14, and these are presented in Fig. 15. We have already seen from Figs. 3 and 4 that the 4-day stratospheric forecast is accurate at both 50 and 10 mb, whereas the 8-day forecast is substantially worse at 50 than 10 mb. Figure 15 shows that even by day 4 a marked error was present in the troposphere, the forecast flux

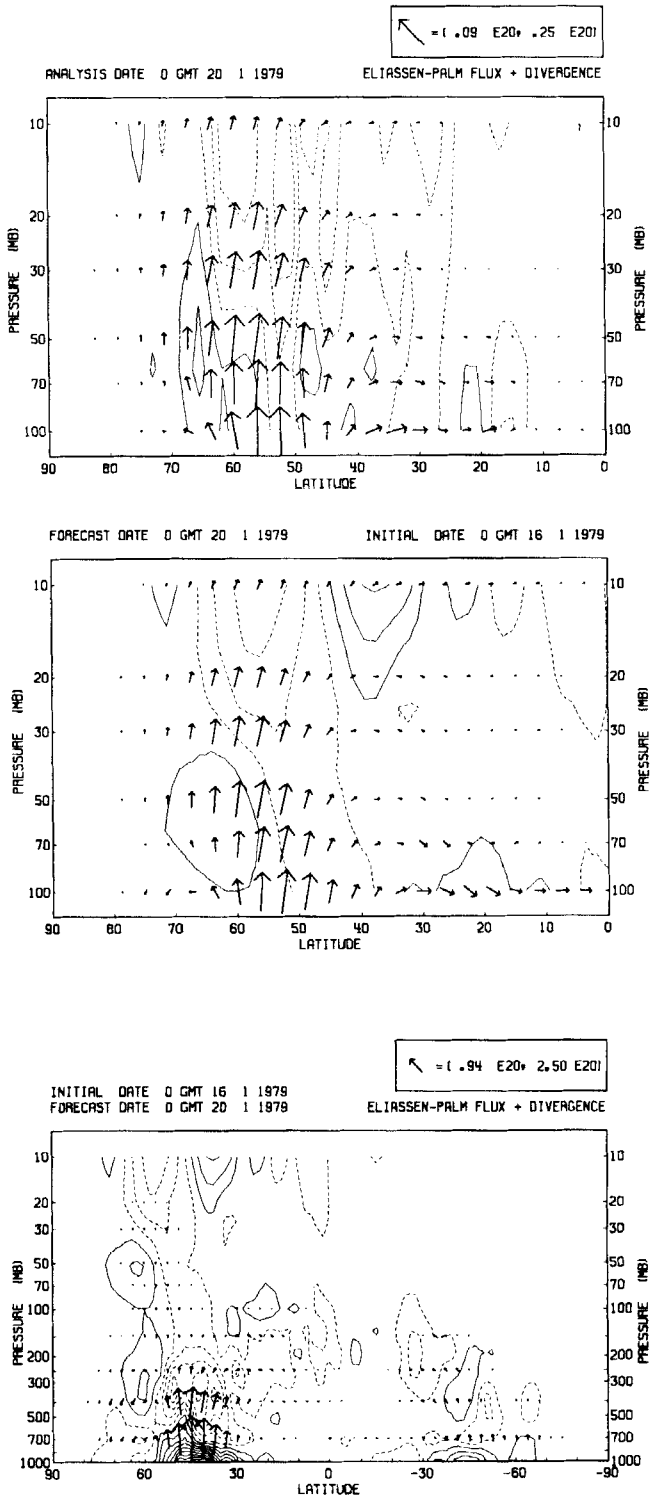


Figure 13. Eliassen-Palm cross-sections from the analysis for 20 January (upper) and from the 4-day forecast from 16 January (middle and lower). The scalings of the flux vector (in units of $m^3$ Pa) are shown for the stratospheric and tropospheric/stratospheric sections. The contour interval for the flux divergence is $4\,m\,s^{-1}\,d^{-1}$, and contours are dashed when values are negative.

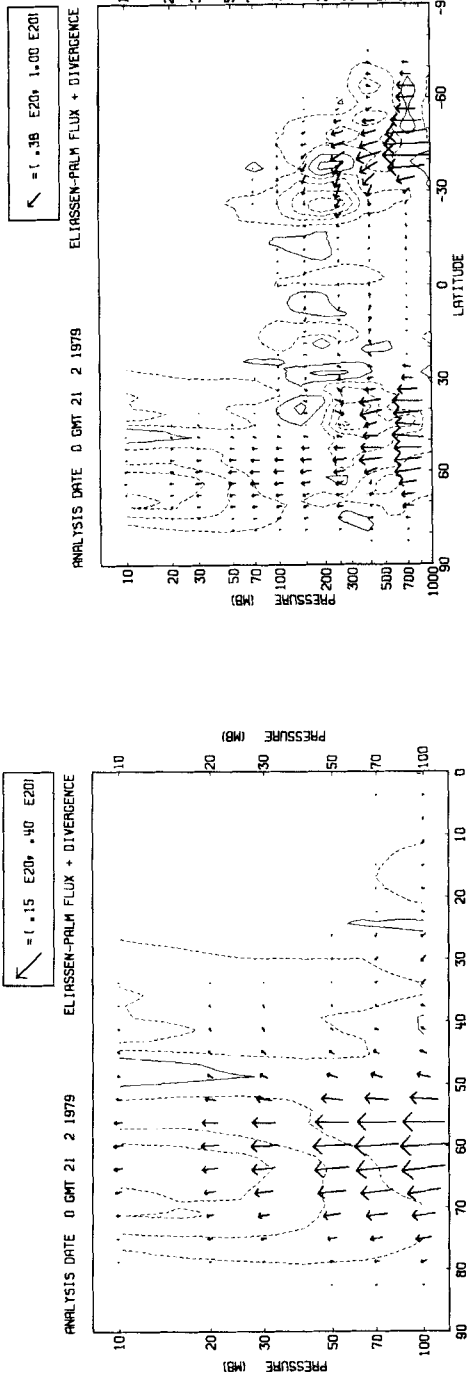


Figure 14. Stratospheric Eliassen-Palm cross-sections from the analysis for 21 February (upper), and from the 4-day forecast from 17 February (lower).

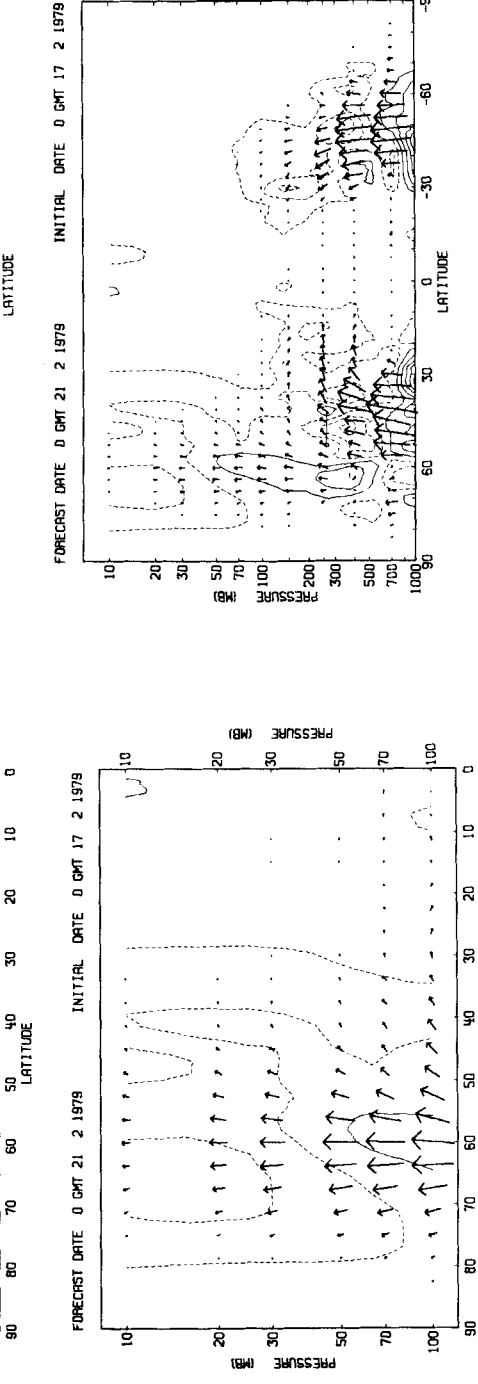


Figure 15. As Fig. 14, but for the combined troposphere and stratosphere.

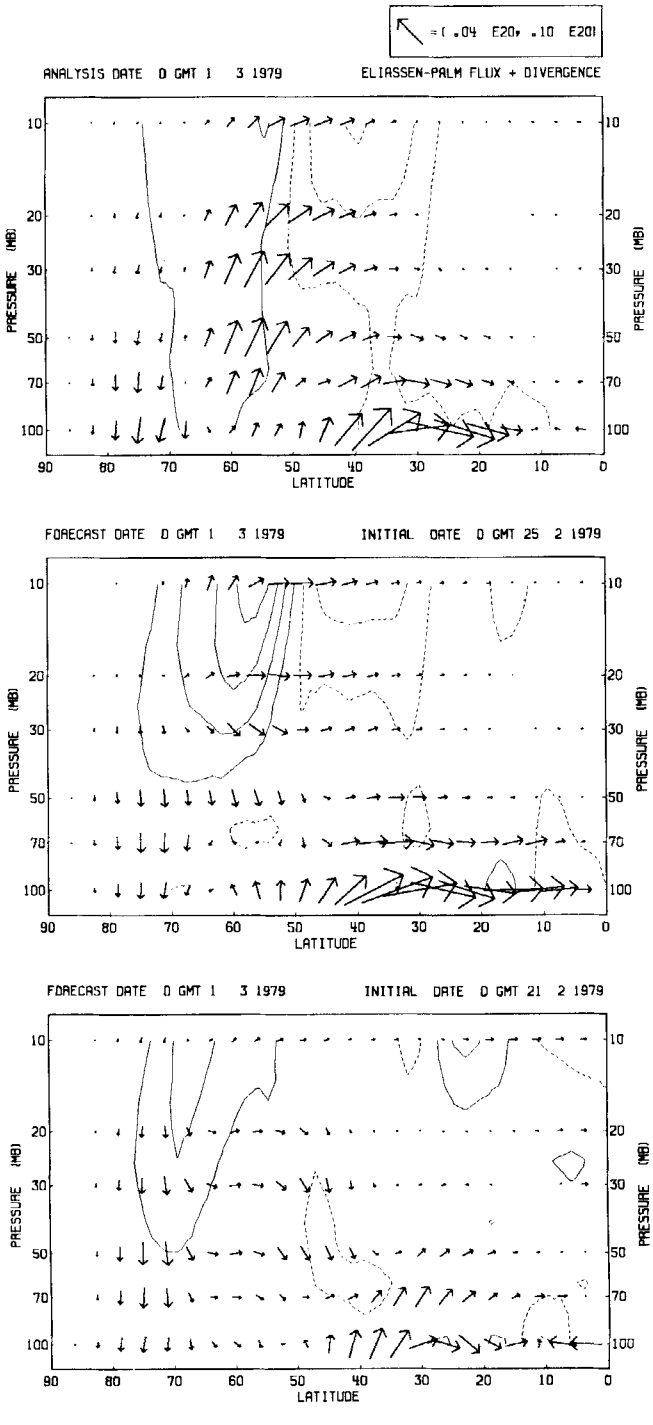


Figure 16. Eliassen-Palm cross-sections from the analysis for 1 March (upper) and from 4-day (middle) and 8-day (lower) forecasts verifying on this date.

at 500 mb exhibiting a too strong equatorward component, with generally too weak amplitude north of 50°N. Examining the detailed evolution of the wavenumber-two component of the geopotential at 60°N for various levels has clearly shown that an erroneous weakening of its amplitude spreads upwards from the troposphere into the stratosphere.

The final sections we present are in Fig. 16, and they show the analysis for 1 March, during the re-establishment of the westerly circulation, together with 4- and 8-day forecasts for this date. Fluxes are generally weaker at this time, and the analysed upward component peaking between 50° and 60°N is completely missed in both forecasts. Both are, however, successful in representing the downward flux component north of 65°N, and the 4-day forecast captures a relatively strong equatorward component, at least at the topmost levels. Synoptically, this corresponds to the marked horizontal tilt of the pressure pattern noted in reference to Fig. 9. Divergence of the flux in the middle stratosphere north of 55°N is found in the forecasts and the analysis, although magnitudes vary.

### (*d*) *Poleward gradients of potential vorticity*

A clear discussion of the likely dynamics of the major 1979 warming has been given by McIntyre (1982), drawing largely on the work of Butchart *et al.* (1982). It is not intended here to contribute in substantial further detail to this discussion, but one additional point of interest has arisen from calculations (for forecasts and analyses) of northward gradients of quasi-geostrophic quasi-potential vorticity (subsequently referred to simply as potential vorticity) and of the related refractive index for the dominant zonal wavenumber 2.

The forementioned authors (and also O'Neill and Youngblut (1982) in the context of the January 1977 warming) discuss the possible importance of the large values of the potential vorticity gradient which occur close to the pole when a strong, narrow polar-night jet is similarly located. These values may lead to a maximum of the refractive index in this region, and thus to a tendency for a focusing towards the polar cap of planetary waves forced from below. The possibility that reflection from a critical layer situated to the south of the polar night jet may help maintain the focusing is also discussed.

Calculations of the potential vorticity gradient are presented here for the form

$$\frac{1}{a} Q_\theta = \frac{\Omega}{a}\left[2\cos\theta - \frac{1}{a\Omega}\frac{\partial}{\partial\theta}\left\{\frac{1}{\cos\theta}\frac{\partial}{\partial\theta}(\bar{u}\cos\theta)\right\} - \frac{4a\Omega}{R}\sin^2\theta\,\frac{\partial}{\partial p}\left(\frac{p}{S}\frac{\partial\bar{u}}{\partial p}\right)\right] \qquad (4)$$

suggested by Hollingsworth *et al.* (1976), where $\bar{u}$ is the zonal-mean zonal wind and $\Omega$ the earth's rotation rate. Its computation involves second derivatives with respect to latitude and height (here computed using simple finite-difference approximations), and as such this computation places constraints on the smoothness of the analysed or forecast fields being used. Nevertheless, reasonably smooth and temporally consistent values have been obtained from the forecasts. Coming as they do from a dynamically-consistent model with a relatively fine (1·875°) horizontal resolution and relatively weak horizontal diffusion, values from the early days of the forecast represent perhaps one of the most reliable current estimates of actual distributions, difficulties associated with irregular distributions of observations being avoided.

The forecast gradients and refractive indices generally confirm the published discussions referred to above, and we present just one figure, from the stage prior to the wavenumber two warming. Figure 17 shows the poleward potential-vorticity gradient computed from the two- and four-day forecasts from 9 February. During this time, as discussed for Fig. 11, there was a substantial acceleration of the westerly zonal-mean flow. Figure 17 shows the development of a strong maximum in $Q_\theta$ between 70° and 80°, a development consistent with the subsequent wave-focusing discussed earlier.

McIntyre (1982) has already suggested that potential vorticity gradients in middle latitudes were weak in mid-February. This is more than confirmed by Fig. 17, and indeed

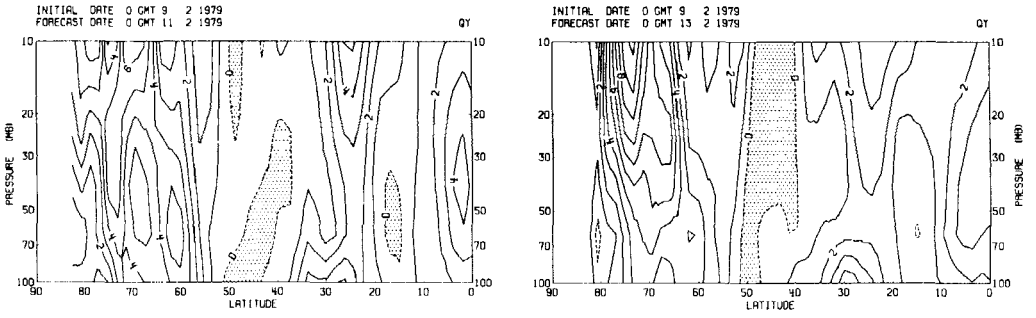


Figure 17. Cross-sections of the northward gradient of the quasi-geostrophic quasi-potential vorticity of the zonal-mean state, as given by Eq. (3). The gradient is non-dimensionalized by a factor $\Omega/a$, and the contour interval is 1 unit. Negative values are shaded. Values are not shown close to the pole where the calculation becomes unreliable.

by a number of other such sections. In fact, in middle latitudes there are deep regions in which zonal-mean potential vorticity gradients become negative, these arising from a marked change in the horizontal shear of the zonal-mean flow at the southern limit of the jet. Such regions would be expected to enhance wave reflection and the focusing in the polar stratosphere. They also raise the possibility of dynamical instability of the polar night jet (Charney and Stern, 1962), although all evidence in this case points to the wavenumber two disturbance as being primarily forced from below.

### (e) *Zonal-mean temperature*

We conclude the presentation of the stratospheric forecasts with a brief discussion of one of their poorer aspects, namely their zonal-mean temperature distribution. Figure 18 presents an indication of systematic stratospheric temperature errors for forecasts from 16 January and 17 February. The upper figures show the analysed changes over the following 8 days. The marked polar warming, by over 30 K at 10 mb, is evident in the February case.

The middle figures show cross-sections of the day-8 error in the forecasts of zonal-mean temperature. These are substantially less in polar regions than the observed changes in the February case, showing the sudden polar warming to have been captured by the model, although it is underestimated in the lower stratosphere, a result consistent with the early re-establishment of the westerly circulation evident at 50 mb in Fig. 4. In the tropics and subtropics, however, there is a substantial erroneous cooling of the model, amounting close to the equator to almost $3\,\mathrm{K\,d^{-1}}$ at 30 mb (the second model level from the top).

Further diagnosis has shown this error to be associated with a too-large radiative cooling at the second model level. The radiative parametrization scheme adopted here is the standard ECMWF scheme, which while coded for arbitrary distributions of model levels, was designed and tested for tropospheric forecasting with a top level generally close to 25 mb. Investigation of its deficiency when the top level is raised is continuing.

The lower plots in Fig. 18 present corresponding forecast results when the ECMWF radiation scheme is replaced by one kindly made available by the Geophysical Fluid Dynamics Laboratory, Princeton. The latter scheme is in fact that used by Miyakoda *et al.* (1970) in their first attempt at prediction of a sudden warming, and it was implemented here by interpolating input fields and computed radiative coolings to and from the 9 levels of the GFDL model. It is clear that with this radiation scheme the erroneous tropical cooling disappears. Use of the scheme also results, however, in an underestimation of the warming of the polar stratosphere, and results are thus less suited to our present purpose of discussing events predominantly confined to this region.

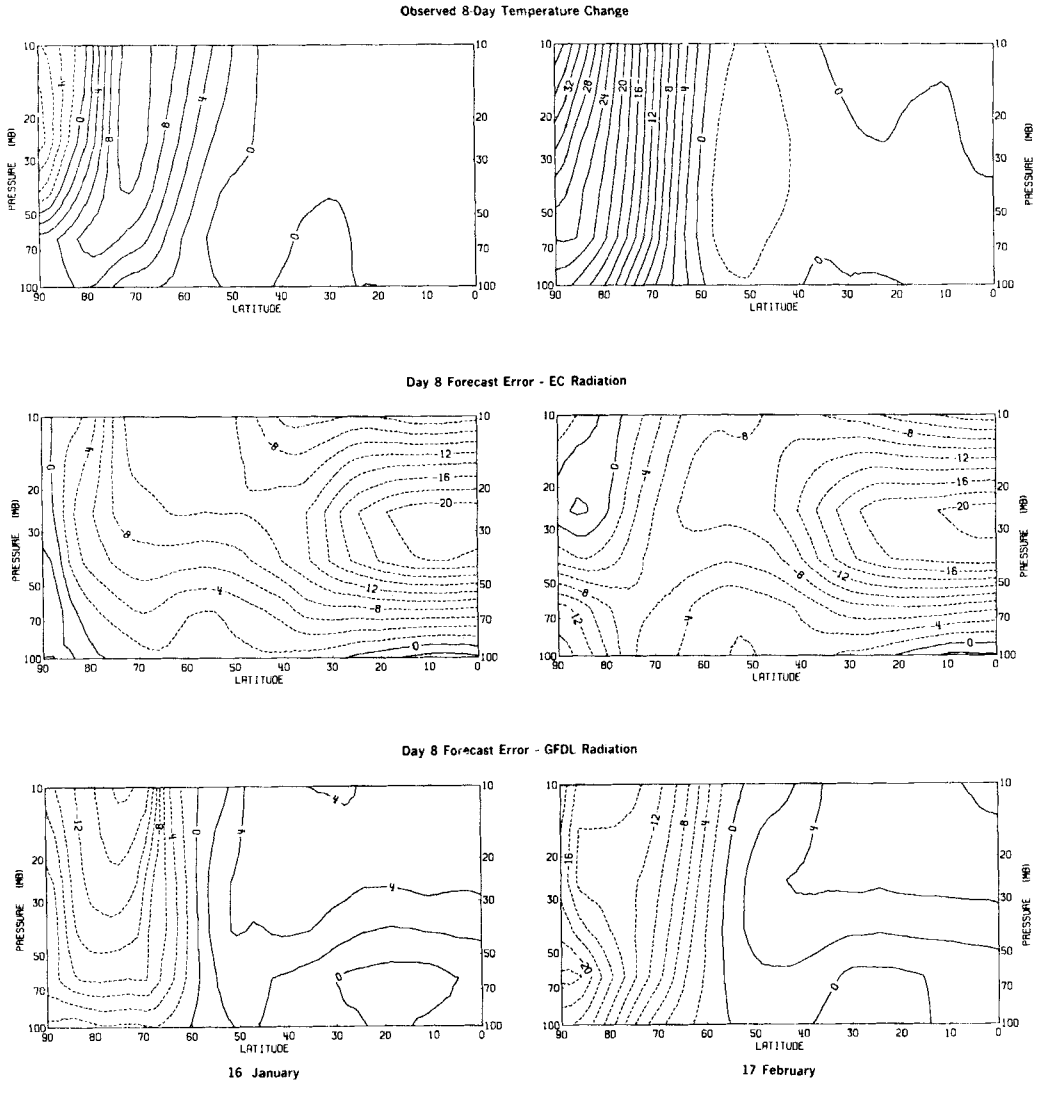


Figure 18. The change in zonal-mean temperature (K) in the 8 days following 16 January (upper left) and 17 February (upper right). The middle and lower plots show day-8 forecast errors for forecasts from these two dates. The contour interval is 2 K.

## 5. The sensitivity of tropospheric forecasts to aspects of the numerical representation

### (*a*) *Stratospheric resolution*

A number of authors, among them Lindzen *et al.* (1968), Nakamura (1976), Kirkwood and Derome (1977) and Bates (1977), have argued that erroneous planetary-wave reflection due to the misrepresentation of the upper boundary condition that inevitably

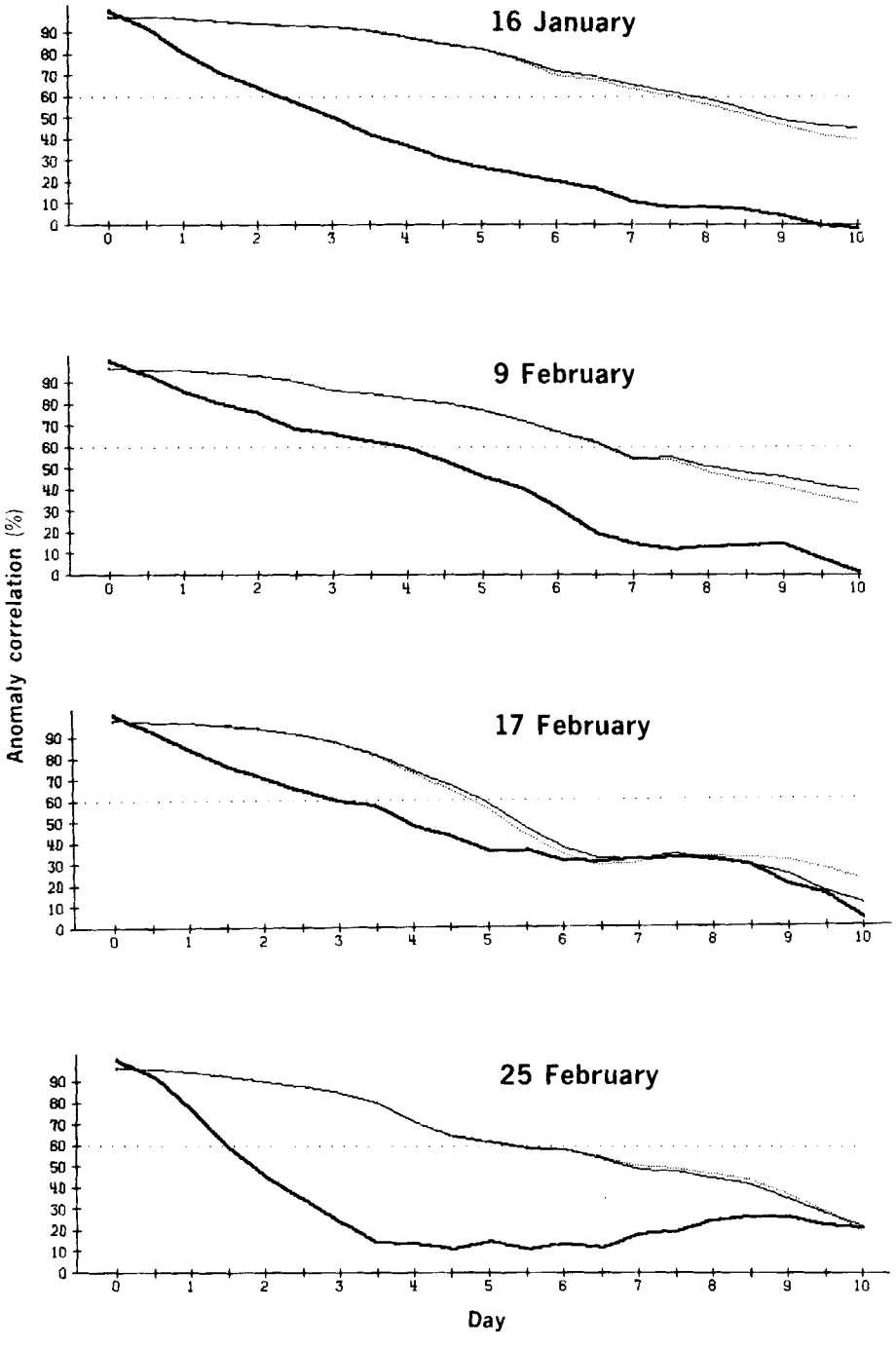


Figure 19. Anomaly correlations of height (%) calculated for the area from 20°N to 82·5°N using heights of standard pressure levels between 1000 and 200 mb. The initial dates of the forecasts are shown. For each date, the heavy solid line indicates a persistence forecast, the light solid line the numerical forecast with a 50 mb top level, the dashed line the forecast with $p_1 = 25$ mb and the dotted curve the forecast with $p_1 = 10$ mb.

occurs in numerical models such as that used in this study may seriously influence the quality of a tropospheric forecast or simulation. Conversely, the Eliassen-Palm cross-sections shown earlier exhibit fluxes which decrease significantly with height in the stratosphere, and whose amplitudes at 10 mb are negligible compared with those in the lower troposphere. This suggests that tropospheric results may be relatively insensitive to stratospheric resolution.

To investigate this question further, hybrid-coordinate forecasts from 16 January, and from 9, 17 and 25 February, have been repeated using the 14- and 16-level resolutions illustrated in Table 1 and Fig. 1. We thus compare results obtained using top full levels at 10, 25 and 50 mb. It should be noted that any differences found are not necessarily due solely to the different location of the top model level. For reasons of accuracy and stability of the finite-difference calculations, layer thicknesses have been chosen to vary smoothly, and the lower the top model level is, the coarser also is the resolution in the vicinity of the tropopause. In addition, we have already noted that the performance of the radiative parametrization worsens as the top level is raised.

The above considerations are not of major importance, however, as the principal result of this aspect of our study is that forecasts are largely insensitive to the changes in resolution examined. This is summarized in the objective measures of forecast skill presented in Fig. 19, which shows correlations of observed and forecast anomalies of the height field, computed for most of the extratropical troposphere of the Northern Hemisphere. This measure has generally been found to give a reliable overall indication of forecast quality, although care must be taken not to place too much reliance on just one such method of assessment, particularly when small samples of forecasts are involved. An anomaly correlation of 50 or 60% is generally used to define a limit of useful predictability (Hollingsworth *et al.*, 1980; Bengtsson and Simmons, 1983).

Figure 19 shows that the four cases are associated with different levels of accuracy for the tropospheric forecasts. The relatively poor performance in the 17 February case has already been noted, while the 16 January case is above average, of a quality attained operationally in some 10% of cases (Bengtsson and Simmons, 1983). The other two cases are closer to the usual accuracy of the ECMWF system for winter cases.

The anomaly correlations obtained using the three different stratospheric resolutions are evidently very similar, particularly for correlations above 50 or 60%. This is especially the case for the poorer forecasts from 17 and 25 February. For the other cases, the forecasts with 25 and 10 mb top levels are very similar up to day 7, and the forecast with the 50 mb top level somewhat different, being clearly worse from day 3 onwards in the 9 February case, but better beyond day 5 for 16 January. In the latter case, the forecast with the 10 mb top level exhibits a relative improvement towards the end of the forecast period, as indeed it does in two of the other three cases.

Synoptic examples of the similarity of forecasts will be discussed in the following sub-section. For the present, we note that the objective verification refers to almost all of the extratropics, and to all scales of motion up to zonal wavenumber 20. Restriction of attention to low wavenumber components closer to the polar region reveals more sensitivity.

This is illustrated by Fig. 20, which shows the amplitude and phase of the wavenumber one component of the geopotential at 60°N for analyses for 20 and 24 January, and for various 4- and 8-day forecasts from 16 January. At day 4 the deficiency of the forecast with the 50 mb top level is evident above 500 mb, while at day 8 it gives a low-level forecast distinctly different from the other three shown, although this forecast happens to be the more accurate.

The accuracy of the phase forecast up to 10 mb that is shown in Fig. 20 is striking. In particular, there is very little tendency for the underestimation of phase tilt at upper model levels that would be expected if substantial erroneous wave reflection were taking place. Such a feature may, however, be noted for the lower resolution forecasts, particularly that for the 50 mb top level.

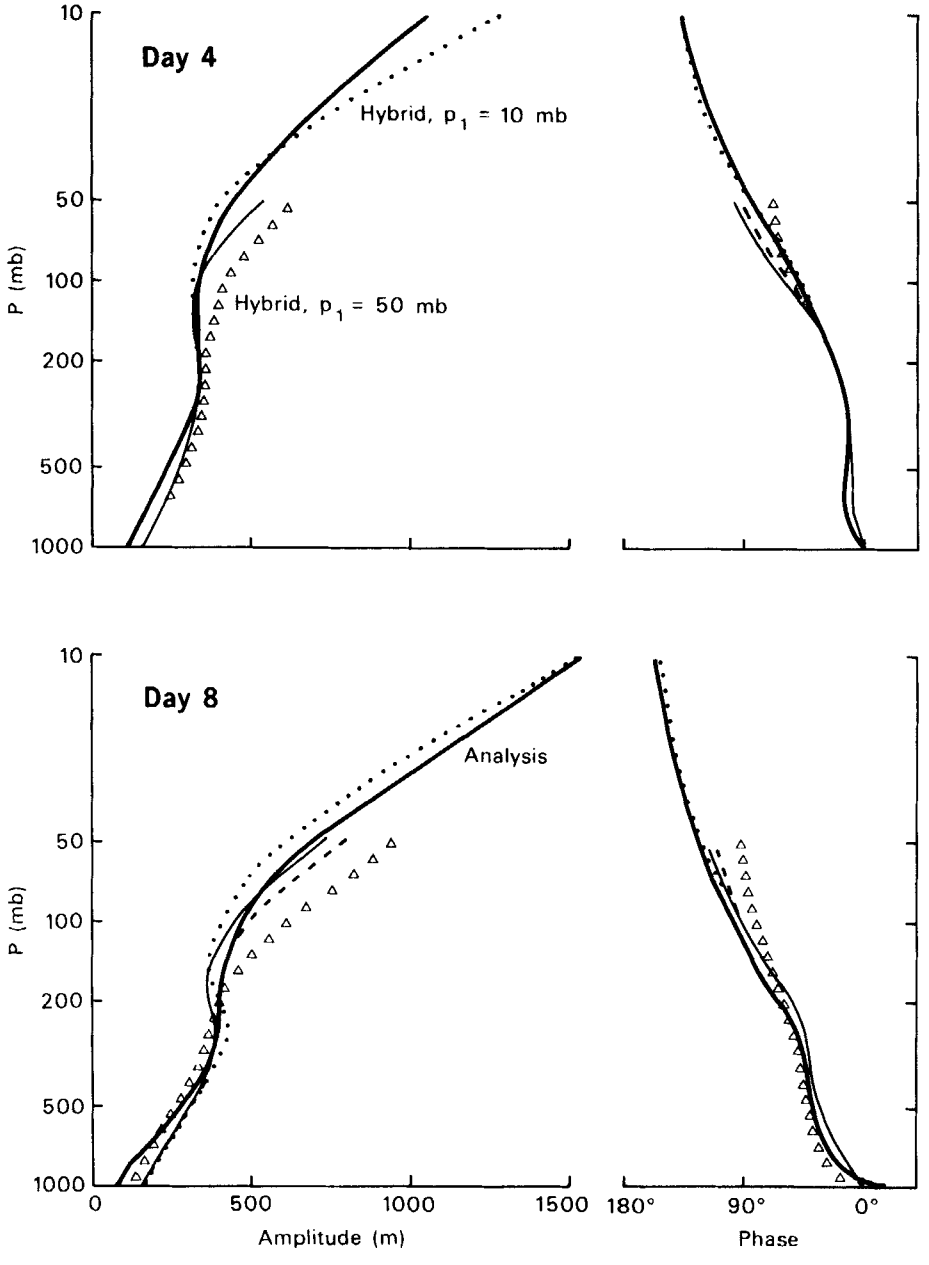


Figure 20. The amplitude and phase of the zonal wavenumber one component of the height field at 60°N for day 4 and day 8 of the forecasts from 16 January. The heavy solid line refers to the analysis, the light solid line to a sigma-coordinate forecast, the dotted line to the hybrid forecast with $p_1 = 10$ mb, the dashed line to the hybrid forecast with $p_1 = 25$ mb, and the triangles to the hybrid forecast with $p_1 = 50$ mb. Hybrid-coordinate curves are not drawn where they are indistinguishable from the sigma-coordinate curves.

*(b) Differences between sigma- and hybrid-coordinate forecasts*

The 16-level forecasts performed using the hybrid coordinate with a 25 mb top level have been repeated using the usual sigma coordinate, with coordinate surfaces coinciding for a surface pressure of 1013·2 mb. The sigma-coordinate forecast from 16 January is

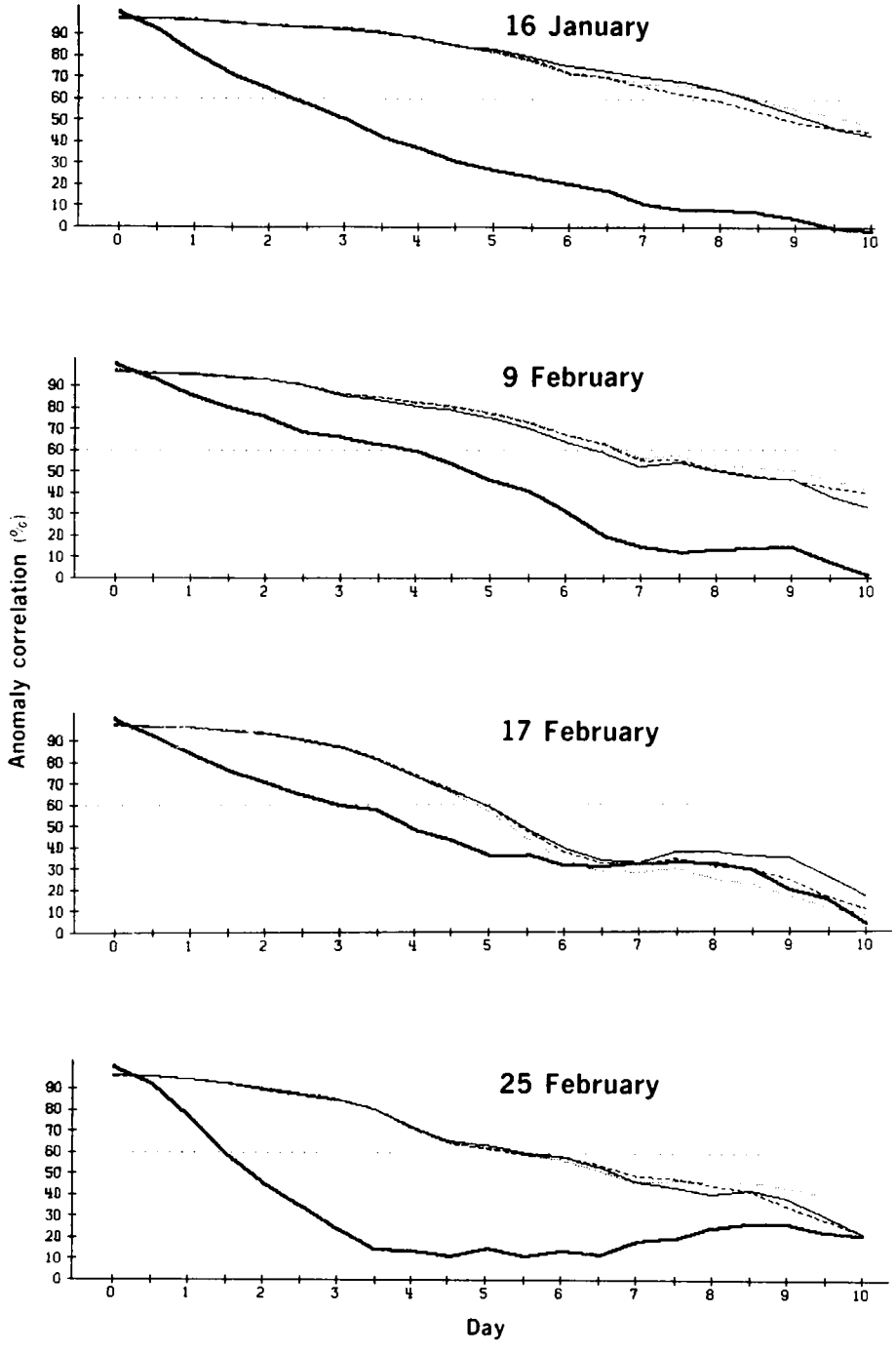


Figure 21. Anomaly correlations of height as in Fig. 19, but for hybrid-coordinate (light solid) and sigma-coordinate (dotted) forecasts.

included in Fig. 20, where it may be seen to be generally closer to the corresponding hybrid forecast than either is to the hybrid forecasts with lower and higher top full levels.

This result is confirmed by comparing Fig. 19 with Fig. 21. The latter figure presents the same objective verification as the former, but for the 16-level sigma- and hybrid-coordinate forecasts. Differences are indeed smaller than in Fig. 19. Two cases give essentially identical results as long as correlations remain above 60%, while the other two slightly favour the hybrid coordinate during this period. Of two other cases examined by Simmons and Strüfing (1981) using operational data for 1981, one similarly favoured the

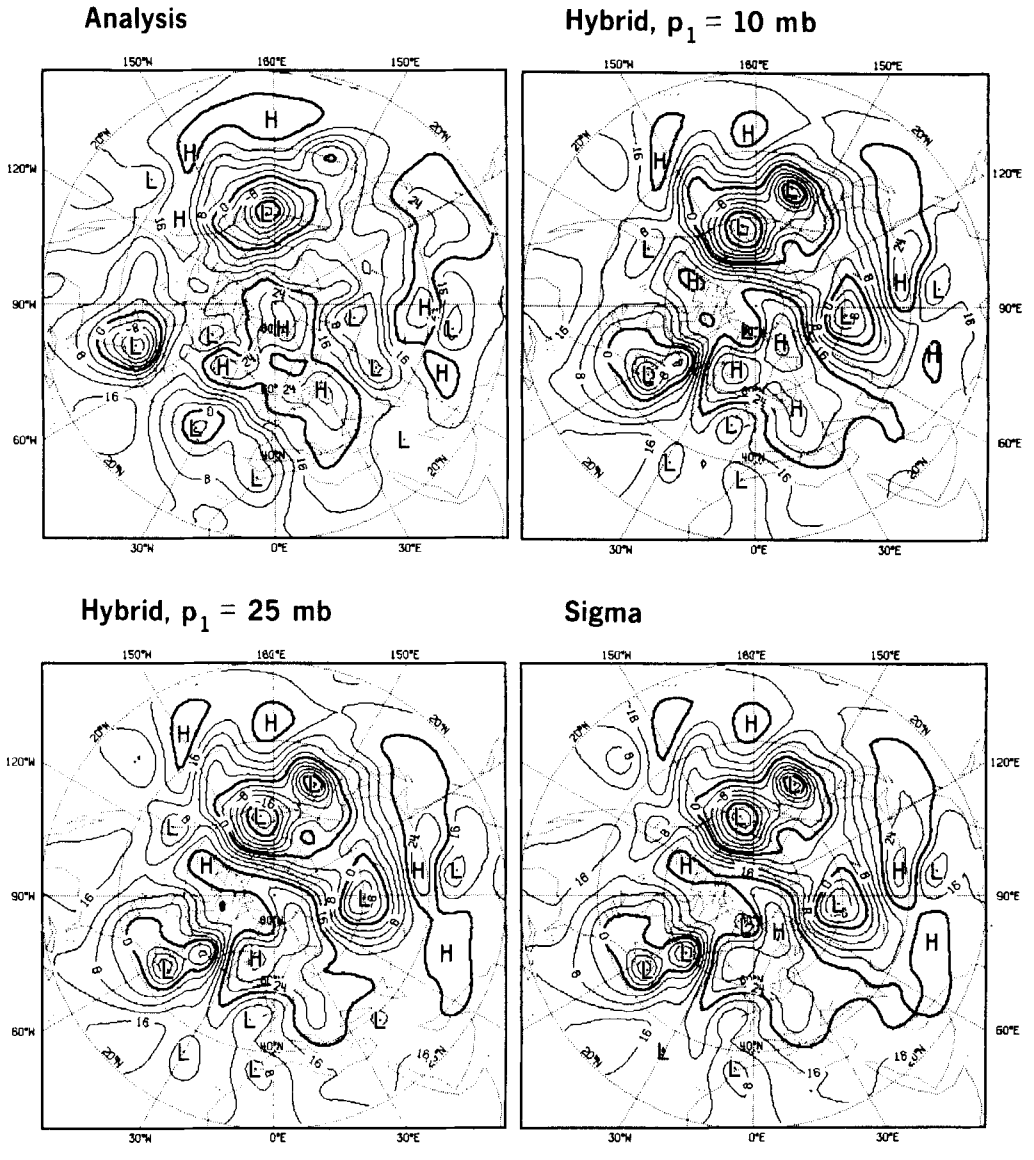


Figure 22. The analysed 1000 mb height for the extratropical northern hemisphere for 22 January (upper left) and corresponding 6-day forecasts from 16 January. The 18-level hybrid forecast is shown upper right and the sigma-coordinate forecast is lower right. The contour interval is 40 m.

hybrid coordinate, while the other (above average) case favoured the hybrid coordinate at days 4 and 5, but the sigma coordinate by day 8.

The overall similarity in forecasts noted using objective verifications in this and the previous sub-section is confirmed by inspection of forecast maps. The case which reveals the most sensitivity in this respect is 16 January, and maps of 1000 mb height at day 6 and 500 mb height at day 8 are presented in Figs. 22 and 23. In these figures the operational FGGE analyses are compared with 16-level forecasts using the sigma and hybrid coordi-

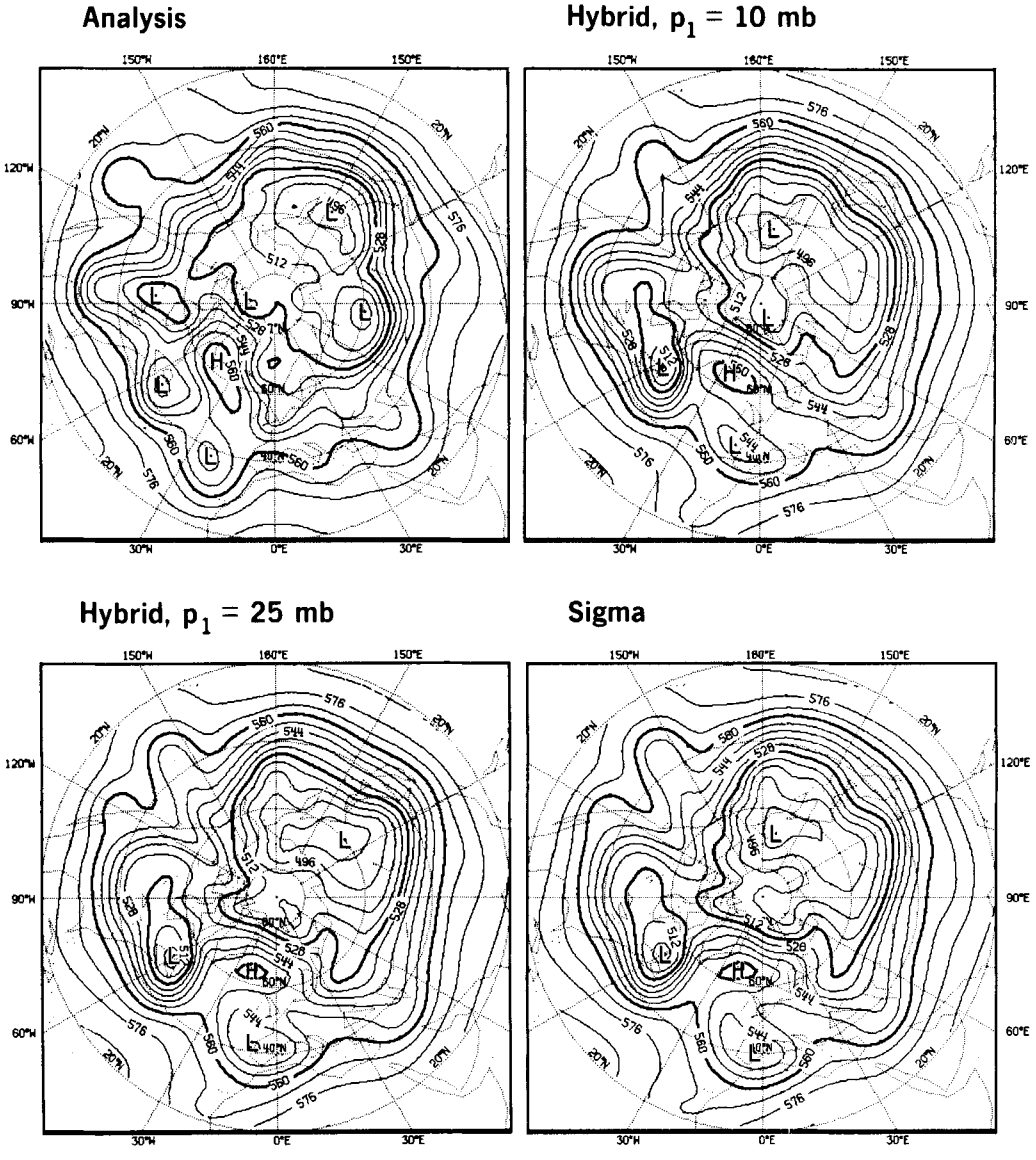


Figure 23. As Fig. 22 but for day 8 forecasts, and the corresponding analysis, of the 500 mb height field. The contour interval is 80 m.

nates and with the corresponding 18-level hybrid forecasts extending to 10 mb. The corresponding objective verification is that shown in the upper graphs in Figs. 19 and 21.

Both figures clearly show the various forecasts to be much closer to each other than any of them is to the analysed state of the atmosphere, but some synoptic differences between them can also be found. Comparing the 18-level hybrid forecast with the 16-level sigma-coordinate forecast we see at day 6 that the former has produced much less of a spurious double-low structure to the disturbance that has developed near the East Coast of North America, and has also produced more distinct high pressure centres over Europe and the North Atlantic. Its improvement over the sigma-coordinate forecast is more marked at day 8, it giving a better phase and orientation to the blocking high in the North Atlantic, to the ridge over the West Coast of North America, and to the three troughs downstream of this ridge. Differences elsewhere are much smaller. At both day 6 and day 8 the 16-level hybrid forecast can be seen to give results intermediate between those for the 18-level hybrid forecast and the sigma-coordinate forecast.

*(c) Alternative hybrid coordinates, and the stability of the semi-implicit time scheme*

In Simmons and Burridge (1981), the idealized properties of an alternative, continuously-varying, hybrid coordinate were examined. The form of this coordinate is more complicated than that described by Eq. (1) of this paper, being given in explicit form by the expression

$$\eta = p/p_s + (p/p_s - 1)(p/p_s - p/p_0) \tag{5}$$

with $p_0$ a constant, here taken to be 1013·2 mb.

Sixteen- and 18-level forecasts have been performed for this coordinate for the two cases exhibiting the most sensitivity in Fig. 21. Results are not shown here since the two alternative hybrid coordinates give very similar forecasts, differences being much smaller than those shown in Fig. 21 for the comparison between coordinate (1) and the sigma coordinate.

It is also worth recording results concerning the stability of the semi-implicit time scheme. It was pointed out by Simmons and Burridge (1981) that implementation of this scheme requires choice of a reference surface pressure, as well as a reference temperature profile, when a hybrid coordinate is used. Care must be taken in the choice of this reference pressure in order to ensure computational stability.

Forecasts using the coordinate given by (5) were successfully carried out using a reference value of 1013·2 mb for the surface pressure. Initial forecasts extending up to 10 mb using the coordinate based on (1) were found, however, to be unstable for such a choice of reference pressure. Thus results given for this coordinate were obtained using an 800 mb reference pressure. The similarity noted above in the results for the two hybrid coordinates strongly indicates that provided computational stability is achieved, the precise choice of reference pressure is not significant. This is in accord with experience regarding the choice of the reference temperature profile (Simmons *et al.*, 1978).

A third hybrid coordinate has also been used in a number of models (e.g. Schlesinger and Mintz, 1979; Fels *et al.*, 1980). This coordinate reduces exactly to pressure above a certain fixed pressure, and is sigma-like below:

$$\begin{aligned} p_{k+1/2} &= p_{I+1/2}\,\eta_{k+1/2}/\eta_{I+1/2}, \qquad k \le I, \\ &= p_{I+1/2} + (\eta_{k+1/2} - \eta_{I+1/2})(p_s - p_{I+1/2})/(1 - \eta_{I+1/2}), \qquad k \ge I, \end{aligned} \tag{6}$$

where $\eta_{k+1/2}$ varies monotonically from 0 to 1 as $k$ varies from 0 to NLEV. For this coordinate, layer thicknesses vary discontinuously in the vertical over high ground.

Idealized analyses described by Simmons and Burridge (1981) indicate that the coordinate given by (6) is more prone to computational instability of the semi-implicit time scheme, and this result has been confirmed in practice. Forecasts from 16 January and 17 February have been performed for this coordinate using an 18-level resolution which is as

given in Table 1 for a surface pressure of 1013·2 mb, and which has an interfacial pressure given by $p_{I+1/2} = 126$ mb, $I = 4$. Both forecasts, however, became unstable after about 5 days of integration using a reference surface pressure of 1013·2 mb. Further integrations on the 16 January case showed the instability to occur also with a reference pressure of 800 mb, and also when the isothermal reference temperature was increased from its usual value of 300 K to 400 K. Further experimentation with this coordinate has not taken place.

## 6. Concluding remarks

It has been shown using case studies from the winter of 1979 that successful forecasts of substantial changes in the stratospheric circulation up to 10 mb may be made for a period of at least 10 days ahead. This occurs despite some systematic deficiencies in the stratosphere of the forecast model, and the evidence from one of the poorer forecasts studied is that the breakdown of the stratospheric forecast follows from an earlier deficiency in the tropospheric forecast. Diagnosis of the forecasts and of the objective FGGE analyses confirms published results for the 1979 winter and provides interesting estimates of the magnitude of the dynamically important poleward gradient of the potential vorticity of the zonal-mean state.

A number of consequences of this ability to forecast stratospheric developments may be identified. One of these, namely the availability of dynamically-consistent data for the verification and extension of observational diagnoses, has already been discussed in this paper. A second, the availability of a model which may be artificially modified to suggest or test hypotheses concerning the important processes involved in the stratospheric warmings, has already been followed up by Butchart *et al.* (1982) in the more restricted, but more controllable, context of a model with a prescribed lower-stratospheric forcing. A third is the possible use of operational forecast data to alert meteorologists interested in stratospheric behaviour, for example those undertaking special observing experiments, to the likelihood of a warming. At the time of writing (January, 1982), a sequence of operational forecasts has just been used to provide such guidance in the case of a partial wavenumber-two breakdown of the westerly vortex at 50 mb (Klinker, personal communication). Finally, it appears that, in these cases at least, the evolution of the warming below 10 mb is not crucially sensitive to conditions in the upper stratosphere and mesosphere.

Tropospheric forecasts have been shown to be largely insensitive to changes in stratospheric resolution in which the top forecast level is varied from 50 to 10 mb. Examination of planetary-wave structures in high latitudes shows some sensitivity, the forecasts with the 50 mb top level exhibiting some distinct, though small, differences from those with higher top levels. Phase variations with height are captured particularly accurately up to 10 mb in the highest resolution calculations, while amplitudes tend to be overestimated at the top model level.

The overall quality of forecasts has also been shown to be largely insensitive to the choice of vertical coordinate. Such differences as have been found generally favour the use of a hybrid coordinate, although caution must be exercised in drawing conclusions from the results of a limited number of cases. It is important to note that in these experiments the hybrid coordinates were not incorporated into the forecast model used in data assimilation cycles. There seems little doubt that use of such coordinates would facilitate the design and implementation of a data assimilation system in which the analysis itself is performed for pressure surfaces, although it is difficult to assess in advance the resulting impact on the accuracy of the forecasts. Overall, there is little evidence to justify a sudden change of an existing model from sigma to hybrid coordinates, but it would appear to be advisable to allow for the possible use of hybrid coordinates by a flexible design of any new system that is to be based on use of a terrain-following vertical coordinate. Such a course is being followed in the preparation of a new forecasting system at ECMWF.

## ACKNOWLEDGMENTS

Thanks are due to the many members of the Research Department of ECMWF who developed the systems which made this study possible, and who subsequently offered advice on points of detail. Stimulating discussions with D. M. Burridge, M. Jarraud and M. E. McIntyre are gratefully acknowledged, as are comments from a referee.

## REFERENCES

Andrews, D. G. and McIntyre, M. E. 1976 Planetary waves in horizontal and vertical shear: the generalized Eliassen-Palm relation and the mean zonal acceleration. *J. Atm. Sci.*, **33**, 2031–2048.

1978 Generalized Eliassen-Palm and Charney-Drazin theorems for waves on axisymmetric flows in compressible atmospheres. *J. Atm. Sci.*, **35**, 175–185.

Arakawa, A. 1966 Computational design for long-term numerical integration of the equations of fluid motion: two dimensional incompressible flow. Part 1. *J. Comp. Phys.*, **1**, 119–143.

Arakawa, A. and Lamb, V. R. 1977 Computational design of the basic dynamical processes of the UCLA general circulation model. *Methods in Computational Physics*, Vol. 17, J. Chang, Ed., Academic Press, 337pp.

Bates, J. R. 1977 Dynamics of stationary, ultra-long waves in middle latitudes. *Quart. J. R. Met. Soc.*, **103**, 397–430.

Bengtsson, L., Kanamitsu, M., Kallberg, P. and Uppala, S. 1982a FGGE four-dimensional data assimilation at ECMWF. *Bull. Amer. Meteorol. Soc.*, **63**, 29–43.

1982b FGGE research activities at ECMWF. *Bull. Amer. Met. Soc.*, **63**, 277–303.

Bengtsson, L. and Simmons, A. J. 1983 Medium range weather prediction – Operational experience at ECMWF. To appear in 'Large-scale dynamical processes in the atmosphere', Ed. B. J. Hoskins and R. P. Pearce, Academic Press.

Boyd, J. 1976 The noninteraction of waves with the zonally-averaged flow on a spherical earth and the interrelationships of eddy fluxes of energy, heat and momentum. *J. Atm. Sci.*, **33**, 2285–2291.

Burridge, D. M. 1979 Some aspects of large scale numerical modelling of the atmosphere. *Proceedings of ECMWF Seminar on Dynamical Meteorology and Numerical Weather Prediction, Vol. 2*, 1–78.

Burridge, D. M. and Haseler, J. 1977 A model for medium range weather forecasting – Adiabatic formulation. *ECMWF Tech. Rep. No. 4*, 46pp.

Butchart, N., Clough, S. A. Palmer, T. N. and Trevelyan, P. J. 1982 Simulations of an observed stratospheric warming with quasi-geostrophic refractive index as a model diagnostic. *Quart. J. R. Met. Soc.*, **108**, 475–503.

Charney, J. G. and Stern, M. E. 1962 On the stability of internal baroclinic jets in a rotating atmosphere. *J. Atmos. Sci.*, **19**, 159–172.

Edmon, H. J., Hoskins, B. J. and McIntyre, M. E. 1980 Eliassen-Palm cross-sections for the troposphere. *J. Atmos. Sci.*, **37**, 2600–2616.

Fels, S. B., Mahlman, D. J., Schwarzkopf, M. D. and Sinclair, R. W. 1980 Stratospheric sensitivity to perturbations in ozone and carbon dioxide: Radiative and dynamical response. *J. Atmos. Sci.*, **37**, 2265–2297.

Grose, W. L. and Haggard, K. V. 1981 Numerical simulation of a sudden stratospheric warming with a three-dimensional spectral, quasi-geostrophic model. *J. Atmos. Sci.*, **38**, 1480–1497.

Hollingsworth, A., Simmons, A. J. and Hoskins, B. J. 1976 The effect of spherical geometry on momentum-transports in simple baroclinic flows. *Quart. J. R. Met. Soc.*, **102**, 901–911.

Hollingsworth, A., Arpe, K., Tiedtke, M., Capaldo, M. and Savijärvi, H. 1980 The performance of a medium-range forecast model in winter – Impact of physical parameterizations. *Mon. Wea. Rev.*, **108**, 1736–1773.

Holton, J. R. 1976 A semi-spectral numerical model for wave, mean-flow interactions in the stratosphere: application to sudden stratospheric warmings. *J. Atmos. Sci.*, **33**, 1639–1649.

Kirkwood, E. and Derome, J. 1977 Some effects of the upper boundary condition and vertical resolution on modelling forced stationary planetary waves. *Mon. Wea. Rev.*, **105**, 1239–1251.

Labitzke, K. 1981 The amplification of height wave 1 in January 1979: a characteristic precondition for the major warming in February. *Mon. Wea. Rev.*, **109**, 983–989.

Lindzen, R. S., Batten, E. S. and Kim, J. W. 1968 Oscillations in atmosphere with tops. *Mon. Wea. Rev.*, **96**, 133–140.

Matsuno, T. 1971 A dynamical model of the stratospheric sudden warming. *J. Atmos. Sci.*, **28**, 1479–1494.

McIntyre, M. E. 1982 How well do we understand the dynamics of stratospheric warmings? *J. Met. Soc. Japan*, **60**, 37–65.

Miyakoda, K., Strickler, R. F. and Hembree, G. D. 1970 Numerical simulation of the breakdown of a polar-night vortex in the stratosphere. *J. Atmos. Sci.*, **27**, 139–154.

Nakamura, H. 1976 Some problems in reproducing planetary waves by numerical models of the atmosphere. *J. Met. Soc. Japan*, **54**, 129–146.

O'Neill, A. 1980 The dynamics of stratospheric warmings generated by a general circulation model of the troposphere and stratosphere. *Quart. J. R. Met. Soc.*, **106**, 659–690.

O'Neill, A. and Youngblut, C. E. 1982 Stratospheric warmings diagnosed using the transformed Eulerian-mean equations and the effect of the mean state on wave propagation. *J. Atmos. Sci.*, **39**, 1370–1386.

Palmer, T. N. 1981 Diagnostic study of a wavenumber-2 stratospheric sudden warming in a transformed Eulerian-mean formalism. *J. Atmos. Sci.*, **38**, 844–855.

Phillips, N. A. 1957 A coordinate system having some special advantages for numerical forecasting. *J. Meteor.*, **14**, 184–185.

Quiroz, R. S. 1979 Tropospheric-stratospheric interaction in the major warming event of January–February 1979. *Geophys. Res. Letters*, **6**, 645–648.

Sadourny, R. 1975 The dynamics of finite difference models of the shallow-water equations. *J. Atmos. Sci.*, **32**, 680–689.

Schlesinger, M. E. and Mintz, Y. 1979 Numerical simulation of ozone production transport and distribution with a global atmospheric general circulation model. *J. Atmos. Sci.*, **36**, 1325–1361.

Simmons, A. J., Hoskins, B. J. and Burridge, D. M. 1978 Stability of the semi-implicit time scheme. *Mon. Wea. Rev.*, **106**, 405–412.

Simmons, A. J. and Burridge, D. M. 1981 An energy and angular-momentum conserving vertical finite-difference scheme and hybrid vertical coordinates. *Mon. Wea. Rev.*, **109**, 758–766.

Simmons, A. J. and Strüfing, R. 1981 An energy and angular-momentum conserving finite-difference scheme, hybrid coordinates, and medium-range weather prediction. *ECMWF Tech. Rep. No. 28*, 68pp.

Temperton, C., and Williamson, D. L. 1981 Normal mode initialization for a multi-level grid-point model. Part I: Linear aspects. *Mon. Wea. Rev.*, **109**, 729–743.

Tiedtke, M., Geleyn, J.-F., Hollingsworth, A. and Louis, J.-F. 1979 ECMWF model-parameterization of sub-grid scale processes. *ECMWF Tech. Rep. No. 10*, 46pp.

Williamson, D. L. and Temperton, C. 1981 Normal mode initialization for a multilevel grid-point model. Part II: Nonlinear aspects. *Mon. Wea. Rev.*, **109**, 744–751.